Centre for Gravitational Physics
Australian National University
Department of Physics
Faculty of Science
0200 ACTON ACT
Australia

White Paper

Adv. LIGO Arm Cavity Pre-Lock Acquisition System

Bram Slagmolen, Glenn de Vine, David Rabeling,
Kirk McKenzie, Adam Mullavey, Daniel Shaddock,
David McClelland, Matt Evans, Yoichi Aso

11 July 2008

LIGO-T080139-00-I

ANU feasibility study for
Advanced LIGO

Contents

1 Introduction

1.1 Purpose of this document

This document proposes methods to aid lock acquisition of the Advanced LIGO arm cavities, and presents a recommendation for future research into these methods.

1.2 Aims of the pre-lock acquisition system

> To control each arm length to a selectable offset–typically ∼10 nm away–from a resonance of the main interferometer beam, with residual arm length fluctuations of ∼1 nm rms or less about that point.

1.3 Overview of the problem

The lowest stage of the quadruple ETM suspensions in Advanced LIGO have electrostatic actuators, which act directly on the test masses. These actuators are chosen because they will deliver lower actuation noise than the voice coil actuators on the initial LIGO test masses. Along with lower noise, these electrostatic actuators will have a lower actuation force on the test masses.

With the predicted velocities of the test masses when freely hanging, the electrostatic actuators, combined with the actuation in the upper suspension chain, will deliver insufficient force to enable routine lock acquisition of the arm cavities [1]. This is unique to the arm cavities, because of the incoherence of the test mass motion at low frequencies between the ITM and ETM, and the required force to acquire lock of the arm.

For routine lock acquisition of the arm cavities, a technique is required to reduce the test mass motion prior to engaging the lock acquisition system to a level where the feedback of the force actuation of the test mass is adequate. The actuation can be to the test mass or other masses in the suspension chain (e.g. penultimate mass).

This system should allow the arm cavities to be brought onto resonance with the pre-stabilized laser (PSL). Developing a system or technique to suppress the test mass motion and to aid lock acquisition is the topic of this paper. A scheme to bring the full interferometer into resonance, starting from the condition mentioned in section 1.2, has been developed and modeled in [2]
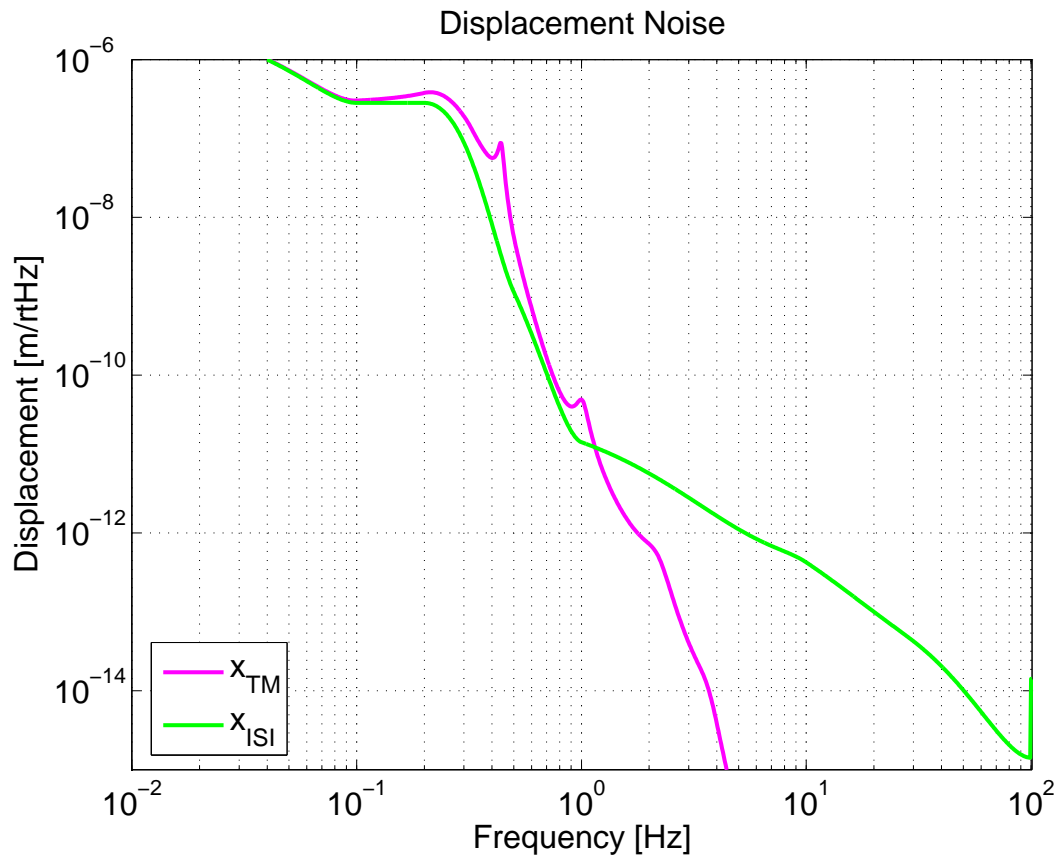
Figure 1.1: Displacement noise of the BSC ISI platform at the quad suspension point and the test mass for comparison.

2 Summary of proposed solutions

Three solutions to aid lock acquisition are discussed in this document. The first solution discussed is a modified version of a **suspension point interferometer** (SPI) [3]. The SPI reduces the test mass motion by sensing and feeding back to the differential motion of the test mass ISI (internal seismic isolation) seismic platforms. The proposed implementation of the SPI for advanced LIGO is introduced in section 2.1 and detailed in chapter 3. The second and third solutions use additional readout techniques to sense the test mass motion directly and feedback to reduce the test mass motion and bring the arm cavities to resonance. The first of these two additional readout techniques is **digital interferometry** (DI) [4]. Digital interferometry is introduced in 2.2 and detailed in chapter 4. The second is **frequency shifted Pound Drever Hall** (PDH) locking [5] which is introduced in section 2.3 and (will be) detailed in chapter 5.

2.1 Suspension Platform Interferometer

The implementation of SPI discussed here uses additional smaller mirrors hung from the ISI platforms of the ITM, ETM and the BS to form a Michelson interferometer with arm cavities, separate to the main interferometer. This SPI could be interrogated using standard readout techniques with either a frequency shifted tap-off of the PSL, or a separate laser phase-locked to the PSL. Once in lock the SPI error signal could be fed back to the ISI platforms to stabilize their differential motion at low frequencies. The lock acquisition of the SPI could be achieved by feedback to the SPI mirrors, which could potentially have a locking bandwidth of ∼100 Hz.

The SPI control system will be required to operated with a tunable dc offset of each of the arm cavities to allow the main interferometer arm cavities to be brought close to resonance before engaging the main interferometer lock acquisition.

The biggest potential advantage of using an SPI to aid lock acquisition is that it may also be operated when the main interferometer is in science mode to prevent ground motion to reach the test masses.

The disadvantages of a SPI in advanced LIGO include: the extra complexity of an separate interferometer, the difficulties associated with hanging optics from the ISI platforms, and the additional optics on the injection benches.

2.2 Digital interferometry

The second solution discussed here is to sense the test masses directly using digital interferometry [4] and feedback to them to suppress their motion. The implementation of DI does not require any additional optical components in the main IFO path. The

probe beam is injected into the system using the faraday isolator at the anti-symmetric port (AS), and detection is done at the ETM transmitted port.

Digital interferometry offers the following advantages:

- no invasive in-vacuum change to the IFO optical lay-out.

- The error signal is linear over an extremely large range.

- The ability to locate the interferometer mirrors to lock point.

The implementation of DI proposed here uses a phase locked, frequency shifted (by GHz) auxiliary laser injected into the faraday isolator at the AS port in the orthogonal polarization to the PSL, see figure 4.3. The sensing of the DI is performed at the ETM transmitted port, with the main interferometer beam separated from the DI beam using polarization and a frequency selective element. The DI error signal would be fed back to the ETM suspension chain. Digital interferometry has been experimentally tested and demonstrated in a proof-of-principal experiment, with a broadband white noise floor of sub-nm/$\sqrt{\text{Hz}}$.

2.3 Frequency shifted Pound-Drever Hall locking

The third solution discussed is to sense the test mass motion using the PDH locking technique also using a frequency shifted laser. The auxiliary laser would be injected into each arm cavity through the ETM. To acquire lock, the error signal would initially be fed back to the auxiliary laser frequency. Once in lock, the actuation could be handed off to the test mass actuators. With the test mass motion suppressed to the required level, the arm cavities can be brought onto resonance with the PSL by tuning the auxiliary laser frequency. The feedback will be similar as for the DI case, and has the advantage of no major in-vacuum change of the IFO optical lay-out.

The auxiliary laser can be of a second wavelength (other than 1064 nm), and minor changes to the optical coating of the ITM and ETM can be made to create a moderate finesse cavity for this wavelength. This modified coating is currently under investigation.

3 The Suspension Platform Interferometer

One approach for implementation of the SPI is an arm cavity Michelson interferometer to sense and feedback to the ISI platforms of the ITMs and ETMs at frequencies up to ≈10 Hz. The SPI mirrors will be located in the arms, while the SPI beam splitter will be co-located to the main IFO beam splitter.

3.1 Concept and Optical Layout

The SPI would have frontal modulation and readout at the dark port. The arm cavity mirrors are suspended from the ISI platforms. Initial lock of the SPI will be done by feedback to the SPI mirrors, which could potentially have a locking bandwidth of ∼100 Hz. Once lock is acquired low frequency feedback is handed over to the ISI platforms. The ISI locking bandwidth will approximately be 10 Hz.

The SPI will operate in the low frequency range where the ground motion is correlated in the corner station. This can possibly mean that for the LIGO Hanford site, only one SPI needs to be installed, which will provide enough information to be used for feedback to both the H1 and H2 interferometer (both with 4 km long arm cavities).

The optical layout is show in figure 3.1(a). The SPI mirror is located in the space between the penultimate mass and the test mass of the ITM and ETM quad suspension, see figure 3.1(b). As for the beam splitter, one solution is to locate the SPI beam splitter inside the penultimate mass (PM) of the main IFO beam splitter. The SPI beam splitter will need its own sensing and control, independent of the PM.

The required laser power is less then a milliwatt to obtain a displacement noise limit of 10^{-15} m/$\sqrt{\text{Hz}}$. There are a few options for the laser source for the SPI. A tap off from the main PSL beam, before it goes into the input mode cleaner. This beam will already have RF modulation frequencies, which can be used for the PDH locking scheme. The only difficulty will be to mode-match and steer the beam into the SPI. To prevent this beam from interfering with the main IFO beam, an AOM will be used to frequency shift the laser beam by a few hundred MHz.

Another option is to use a separate laser, even with a different color (e.g. 532 nm), to prevent spurious interference with the main IFO beam. With this approach the laser frequency will need to be stabilized to 1 Hz/$\sqrt{\text{Hz}}$ at 1 Hz [6]. This can be done by locking it to the PSL beam. Alternatively a separate reference cavity can be set up, or even a double resonant reference cavity in which the main PSL and the SPI laser are resonant.

With SPI mirror reflectivities of 90%, the finesse of the SPI cavities is about 30, which is sufficient.

(a) The optical lay-out of the SPI interferometer.

(b) SPI mirror suspension implementation.
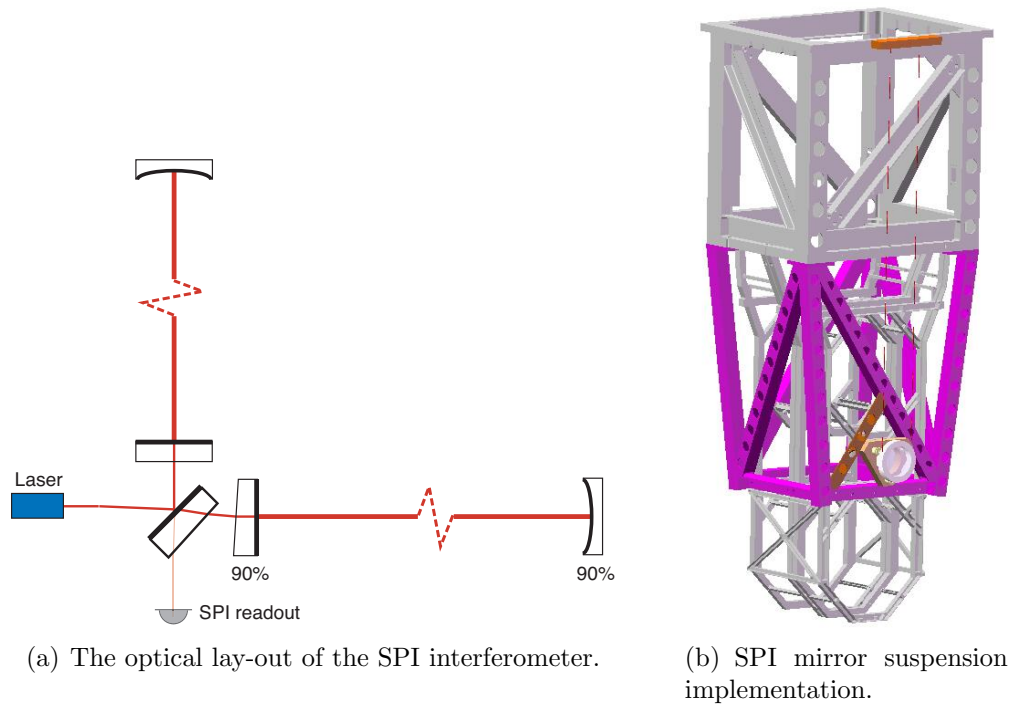
Figure 3.1: SPI arm cavity Michelson interferometer and the SPI mirror suspension implementation onto the Quad suspension.

3.1.1 Single Arm Cavities

An alternative layout is to inject the laser beam from the back of the arms, through the ETM suspension. This will require two separate injection systems, one in each end station. The injection laser will need to be phase locked to the PSL, more detail on how to do this is given in section 5.2.3.

3.2 Implementation

As mentioned before, the SPI mirrors will be a separate suspended optic, hung from the ISI platforms as shown in figure 3.1(b). The optic will be located just before the quad cage, between the test mass and the penultimate mass. (ref. Matt and Dennis). The mirrors will have actuators (OSEMs) for local and global control, see figure 3.1(b).

Minor modifications to the quad suspensions are required to implement the SPI mirror.

3.2.1 SPI Arm Cavities

The SPI mirrors are 5.5 inch in diameter and 1 inch thick, and clamped inside a metal ring to which 3 magnets are glued for sensing and actuation using the OSEMs.

The arm cavity has two curved mirrors, each with an ROC of 4 km. The waist, in the center of the cavity, will be 24 mm. The spot size on mirrors will be 37 mm (radius).
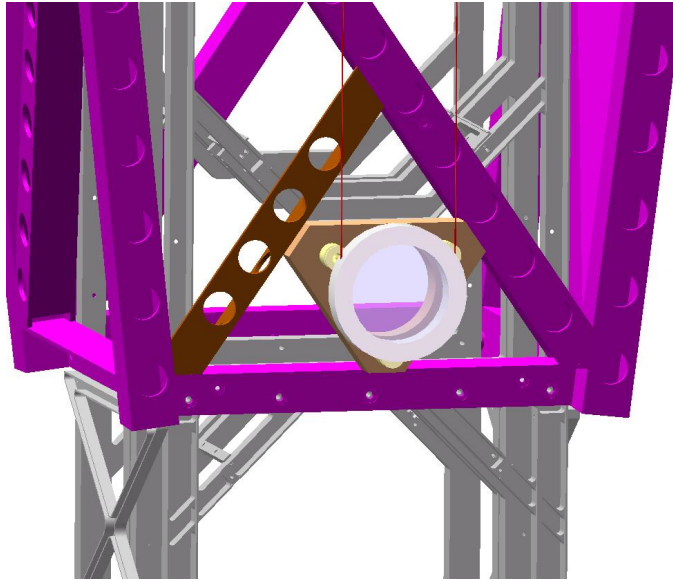
Figure 3.2: SPI mirror suspension implementation.

3.2.2 SPI Beam Splitter

The beam splitter for the SPI is located inside the penultimate mass of the main IFO beam splitter. The SPI beam splitter needs to have its own local control to be able to align the SPI beam independent from the main IFO beam.

3.2.3 Input Optics

A modest pre-mode-cleaner would be sufficient for the beam preparation, prior to launching into the mode-matching optics. TBD.

3.2.4 Readout

The SPI readout will be at the dark port on HAM4, and directed to outside the vacuum, where it will be detected and demodulated.

The SPI beam will be relatively small, so no Beam Reducing telescope will be required. Some 2-inch mode-matching optics may be all that is needed to steer and focus the beam onto the detector.

3.2.5 Feedback Control

The feedback will be to the ISI platform actuators to reduce the test mass motion. As shown in the feedback model ISI feedback bandwidth of ~8 Hz. The SPI mirrors have OSEMs so they can be used to increase the locking bandwidth of the SPI cavities.

3.3 Technical Issues

3.3.1 ISI Tilt Coupling

A potential problem with the SPI is that the tilt of the ISI platform will mimic a longitudinal displacement of the SPI mirror in respect to the test mass.

The current design has the SPI mirror located just in front of the Quad system. This reduces the coupling of the tilt motion of the ISI platform to the longitudinal motion SPI mirror, and will mainly manifest as vertical motion of the SPI mirror. The suspension wire length is 1.35 m, setting a longitudinal resonance frequency of 0.43 Hz, while the test mass longitudinal resonance frequency is 0.44 Hz. In the model, see figure 3.3, the length asymmetry is set to 2 mm ($1.5 \cdot 10^{-3}$ fractional) and is responsible for the resonant peak at 0.43 Hz. Reducing this asymmetry by two, results in approximately half the RMS displacement just before the 0.43 Hz resonance to $\sim 7 \cdot 10^{-10}$ m.

3.3.2 Beam Centering

Mis-centering of the beam on the SPI mirrors will mimic a longitudinal displacement when the mirror tilts due to the motion of the ISI platform. It turns out that although the mis-centering increased the displacement noise, this coupling is not overly sensitive. In figure 3.4, the mis-centering is 3 mm, with an RMS test mass displacement of 1.5 nm. Removing the mis-centering will drop the rms displacement down to 1.4 nm (including a 2 mm wire length asymmetry as discussed in the previous section).

3.3.3 Frequency Stability

With the beam injection in the corner station, the SPI laser can be stabilized to the PSL. The SPI laser needs to be stabilized to the SPI displacement noise floor. Setting this to 10% of the required displacement noise of 1 nm rms, the SPI laser needs to be stabilized to,

$$\delta\nu = \frac{\delta x \; \nu}{L} = \frac{0.1 \cdot 10^{-9} \cdot 2.8 \cdot 10^{14}}{4 \cdot 10^3} = 7 \, \text{Hz rms} \tag{3.1}$$

3.4 Performance

Matlab/Simulink modeling has been done [6], to investigate the possible performance of an SPI system. In figure 3.4 it is shown that the SPI can reduce the test mass motion to 10^{-9} m RMS up to 0.4 Hz, after which it drops down and follows the test mass motion at frequencies above 1 Hz.

3.5 Risk Assessment

The SPI can be an independent subsystem, and would be able to run when ever it is required. It potentially can be running during science mode, possibly improving the low frequency band of the detector.
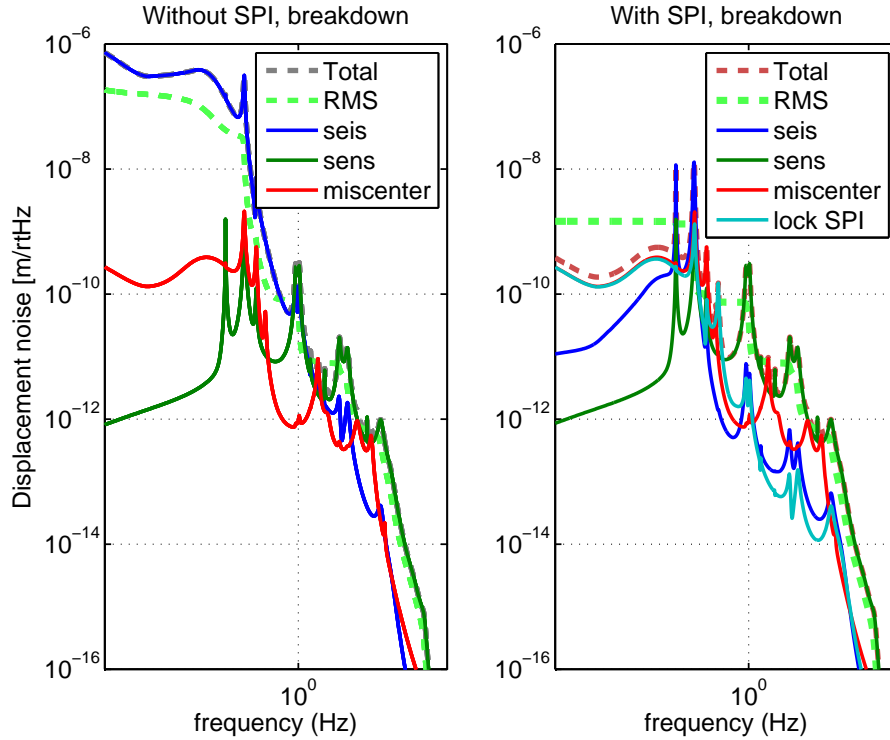
Figure 3.3: Breakdown of the modeled SPI noise budget. In here the suspension wire asymmetry is set to 2 mm and the beam mis-centering on the mirror is 3 mm.

The implementation is very invasive, not only for the actual SPI mirrors as well as the injection optics inside the vacuum system.

3.6 SPI Summary

Initial modeling shows that the SPI meets the displacement suppression requirement in the frequency band up to 1 Hz. In addition, the SPI can be running full time, even during science mode. This is possible as there is no mechanical or optical interference between the main interferometer and the SPI. Alternatively the feedback can be turned of and activated when a threshold displacement is observed. This is to keep the main interferometer locked, prior to going back into science mode, increasing the up time.

A draw back is that there are major in-vacuum modifications required. These include changes to the Quad suspension cage and changes to the beam splitter penultimate mass to accommodate the SPI beam splitter. The mode-matching optics, which partly will be located on HAM3, will need further investigation. Alternatively, the light can be injected from the end-stations, greatly reducing the in-vacuum modifications. Then only the suspended SPI mirrors are to be installed. The mode-matching and steering the beam into the SPI cavity will need to be further investigated.
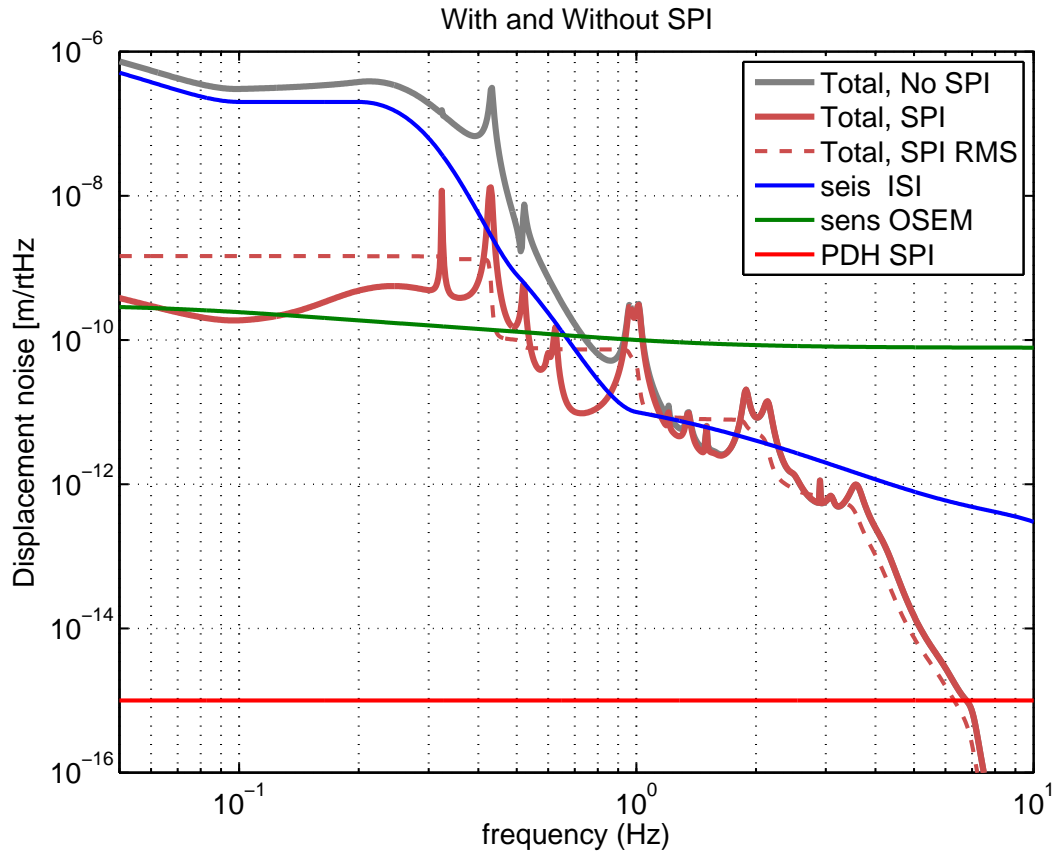
Figure 3.4: Modeled SPI noise budget.

4 Digital Interferometry

Using digital interferometry (DI), the relative displacement of the test masses can be sensed directly. This continuous sensing allows test mass separation to be stabilized by feeding back to the test mass suspension chain. DI's heterodyne interferometry has no specific lock point and can track the position of mirrors over many microns. The technique provides a high update rate compatible with feedback control systems and can be readily extended to readout the positions of more optical components if necessary to aid in acquiring other degrees of freedom.

4.1 Measurement Concept

DI employs a digital pseudo-random noise (PRN) code phase-modulated onto the light source, which allows optical signals to be isolated based on their delay. This signal isolation capability allows multiple optical components to be measured using a single metrology system.

Consider the optical layout shown in figure 4.1 for the case of three partial reflectors: A beamsplitter divides the laser output into a local oscillator and probe beam. The local oscillator is frequency-shifted by an acousto-optic modulator (AOM) to provide a heterodyne signal at the photodetector with a frequency f_h. A PRN code generator drives an electro-optic modulator (EOM) to produce either a zero or π phase shift on the probe beam before it is directed towards the mirrors. The reflected light is recombined with the local oscillator and the interference signal is measured by the photodetector.

The key difference from a conventional heterodyne interferometer is the PRN phase modulation. With no PRN modulation, the heterodyne signal at the photodetector is determined by the vector sum of the reflections from all three mirrors. Information about the individual mirror positions is lost. With the PRN modulation present, the signal from each mirror will possess a time-varying phase shift unique to its time of flight from the EOM.

The effect of the PRN encoding and decoding on the measured signals is shown in Figure 4.2. For clarity we will consider the encoding and decoding with only the M1 reflection present (e.g. M2, M3 blocked). The first row shows the signal at the photodetector in a conventional heterodyne interferometer. With DI, the PRN code (A) randomly inverts the amplitude of the heterodyne signal at the photodetector producing the chopped sine wave (B). In the processing channel for monitoring M1 (centre column), the photodetector output is multiplied by the PRN code with a matching delay (C1), to recover the full heterodyne signal (D1). The phase of this heterodyne signal gives the mirror displacement x_1. The M2 channel (right column) uses a different decoding delay (C2); in this case the signal is randomly re-inverted (D2)
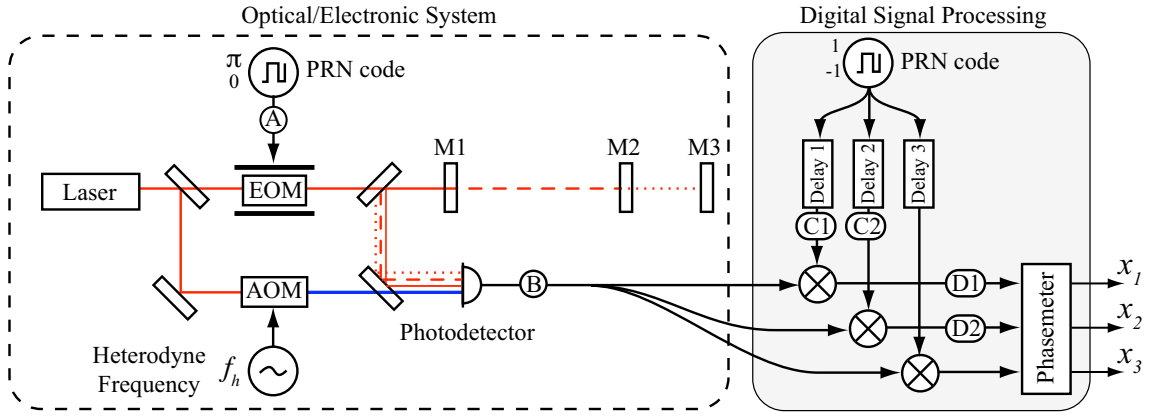
Figure 4.1: Digital Interferometer for monitoring displacements of three mirrors M1, M2, and M3. Each reflection is isolated by matching the decoding delays to the optical delay. Signals measured at points A, B, C1, C2, D1, and D2 are shown in Figure 4.2.

and appears as a broadband noise background to the measurement. This broadband noise can be strongly rejected by appropriate filtering and averaging in the phasemeter. This demonstrates that by adjusting the decoding delay, we can selectively isolate signals based on their total optical/electronic delay.
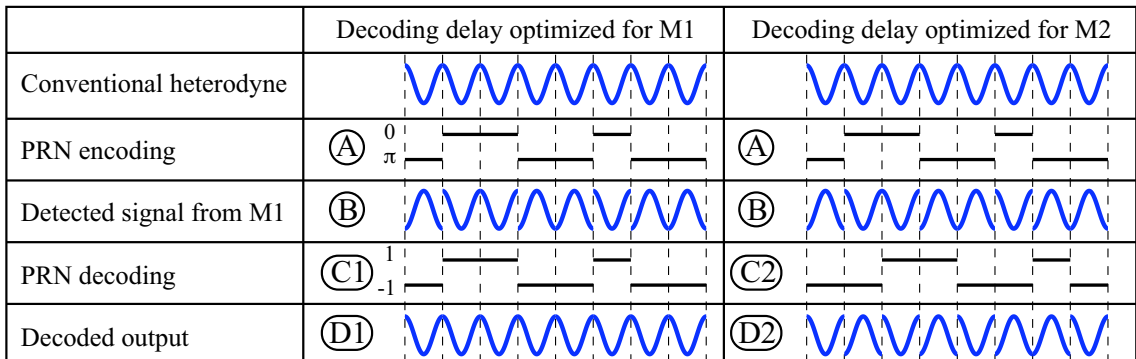
Figure 4.2: Illustration of signals from one mirror (M1) with matched (centre column) and unmatched (right column) decoding delays. Signals A, B, C1, C2, D1, D2 correspond to the measurement points in Figure 4.1. The decoded output is subsequently bandpass filtered to extract the signals; the near pure tone of the centre column will be passed by the filter giving a clear signal for M1, while the noisy signal in the right column will be blocked by the filter and the M1 signal will not contaminate the M2 output.

4.2 Implementation

There are several ways to apply DI to LIGO lock acquisition sensing. It is expected that at this point design will be refined as the impact of different options and the

benefit of additional capabilities are investigated more fully. A discussion of other options and the rationale for deciding between them is deferred to appendix **??**.

4.2.1 Beam Injection

Figure 4.1 presented a reflection based sensing scheme designed for measuring low reflectivity optics. For sensing high reflectivity optics, such as those in LIGO, a transmission based scheme will allow the amplitudes of the different reflections to be more closely matched. Figure 4.3 shows the optical layout for injection and extraction of DI signals in LIGO. The PRN modulated light is injected at the AS port and is detected after transmission through the ETMs. Injection from the AS port has the advantage that all the core optics can be monitored, with the sensing done at both the end-stations. The frequency stabilization (at GHz offset) can more easily be done as the PSL is in close proximity of the DI injection laser. In addition only one DI source is required and the local oscillator (LO) will be delivered to each end-stations by an optical fiber. No further stabilization of the LO in the end-stations is required as the phase jitter is common to all DI measurements measured in each arm.

An alternative option, is to inject using the output crystal of the faraday isolator of the IOO subsystem. It turns out that this is not possible in the current design, as there is no space to inject into the other polarization, because the angle between the ordinary and extraordinary rays is very narrow, hence aligning the DI beam into the crystal will be difficult. Another option is to inject at the POP, and through the PR2 mirror, which will have a 250 ppm transmission. The power of the DI beam, will need to be quite large to obtain a power level behind the ETM of ∼100 pW.

The DI laser will be at 1064 nm wavelength and hence will see the main IFO optics reflectivities. Figure 4.4 shows the power of the DI beam behind the ETMx, while injected at the AS port with 1 W incident on the SRM. The 0th arm cavity transmission is the straight transmission through the ITM and the ETM while the following transmissions are from subsequent roundtrips through the arm cavity. The PRC roundtrip transmission refers to the reflections from the ITM back to the PRM (transmitted through the BS) and back through the ITM and ETM. The SRC roundtrip transmission is analogous to the PRC roundtrip transmission, except it is for the signal recycling cavity (and reflected from the BS).

4.2.2 Back-scatter at the AS port

The proposed injection of the DI beam into the faraday isolator is worrisome, as any light injected back into the interferometer can degrade the detector sensitivity. The DI beam is injected into input PBS of the faraday isolator. By doing this, it will 'open-up' this port for spurious re-injection of the IFO beam leakage reflected back into the interferometer.

Scatter at the AS port has been analyzed in T060303-00 [7]. From section 2.2, equation (3) the motion of the scattering surface should be less than:

$$x_{sc} < \frac{10^{-17}}{\sqrt{R_r}} \text{ m}/\sqrt{\text{Hz}} \text{ , } f > 10 \text{ Hz} \tag{4.1}$$
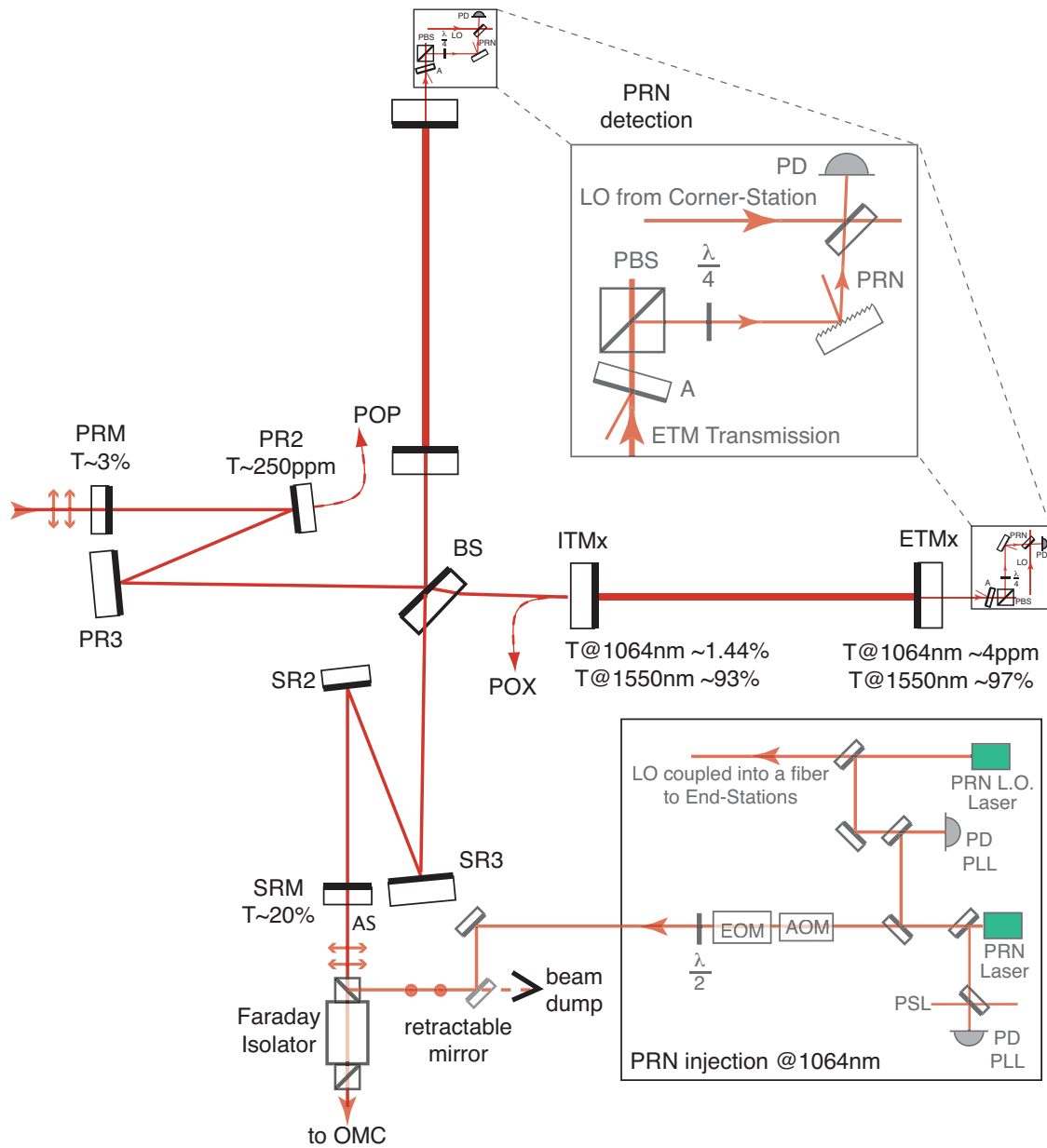
Figure 4.3: DI injection and readout optical layout. The DI beam is injected into the input PBS of the faraday isolator at the AS port. The main IFO is in horizontal polarization (p-polarized), so the DI can be injected into the vertical polarization (s-polarized). This is to separate the DI beam from the main IFO carrier at the readout ports.
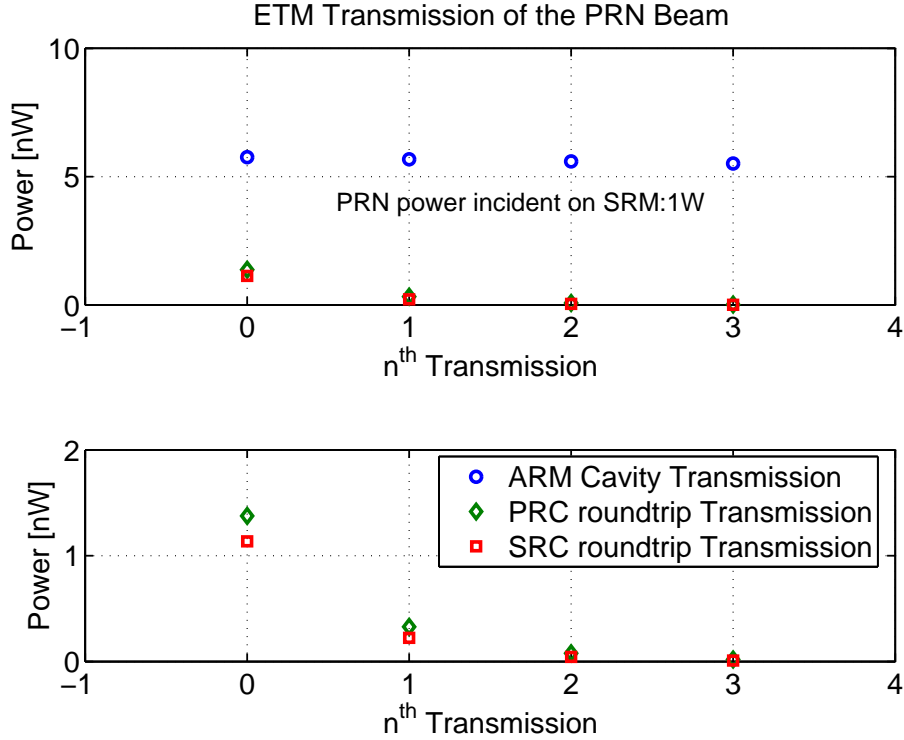
Figure 4.4: The power transmitted through the arm cavity, when injected into faraday isolator. The PRC transmission is incident onto the ITM, and then reflected back from the PRM through the arm cavity. The SRC transmission is reflected from the ITM, and then reflected back from the SRM through the arm cavity. The n=1 transmission for the PRC and SCR is 4.1 pW and 2.7 pW respectively, that is with 200 mW of power transmitted through the SRM (see figure 4.3).

were R_r is the power reflectivity into the interferometer TEM_{00} mode, of the scattering surface. This limit includes a safety factor of 10x.

Also from T060303-00, the factor $R_r = BRDF(\theta) \cdot \Omega_{1/e}$. Behind the SRM, $\Omega_{1/e} \sim 2 \times 10^{-8}$ str^{-1} and the $BRDF(\theta)$ for a 2" steering mirror is $\sim 3 \times 10^{-6}$ str^{-1}, resulting in an $R_r = 6 \times 10^{-14}$.

The motion of the mirror steering the DI beam into the faraday isolator can have a maximum motion of:

$$x_{sc} \quad < \quad 4 \times 10^{-9} \text{ m/}\sqrt{\text{Hz}} \text{ , } f = 1 \text{ Hz} \tag{4.2}$$

$$x_{sc} \quad < \quad 4 \times 10^{-11} \text{ m/}\sqrt{\text{Hz}} \text{ , } f > 10 \text{ Hz} \tag{4.3}$$

in here a $1/f^2$ dependency of frequencies up to 10 Hz is assumed.

Assume the DI beam is steered using a Tip-Tilt mirror mounted on a HAM ISI platform. The transmissibility of a Tip-Tilt at 1 Hz and 10 Hz is 1 and 0.27 respectively (with a bump of a factor of 2 at 2 Hz). The HAM ISI motion at 1 Hz and 10 Hz is 4×10^{-10} m/$\sqrt{\text{Hz}}$ and 4×10^{-11} m/$\sqrt{\text{Hz}}$ respectively (from T060303-00, figure 3). Combining these values gives the motion of the DI steering mirror into the faraday

isolator:

$$x_{TT} = 4 \times 10^{-10} \text{ m}/\sqrt{\text{Hz}} \, , f = 1 \text{ Hz} \tag{4.4}$$

$$x_{TT} = 1 \times 10^{-11} \left(\frac{10}{f} \right) \text{ m}/\sqrt{\text{Hz}} \, , f > 10 \text{ Hz} \tag{4.5}$$

The $1/f$ dependency above 10 Hz is due to the roll-off of the Tip-Tilt mirrors, and indicates that it is feasible to use the faraday isolator as input of the DI probe beam. In addition a retractable steering mirror before the beam dump at the beam splitter port can be used to remove the DI beam entering the AS-port when in science mode.

4.2.3 Detection

The DI readout for each arm cavity occurs at the transmitted port at the ETM, see figure 4.3 for an optical layout. Several stages of isolation are used to adequately separate the DI laser light from the main IFO carrier. The DI beam is injected into the orthogonal polarization from the main IFO carrier. In addition the DI laser has a frequency offset of a few GHz, which allows separation by use of a grating (diffraction grating or fiber Bragg grating). The polarization and frequency offsets prevent saturation of the DI detectors by the IFO beam, of which a -60 dB of optical separation would be sufficient. The final two stages of separation are provided by the limited bandwidth of the photodetector (the beatnote between the LO and the main IFO beam occurs at > 1 GHz) and the decoding of the DI signal (which converts the sinusoidal IFO beatnote to broadband noise).

If the DI detection is all done on the suspended breadboard behind the ETM, then the maximum return power (of the main IFO carrier) can be up to 1% [2].

4.2.4 Synchronization at the end-station

The DI detection is done in the end-stations, where all the digital computation is done as well. The DI demodulation needs to be synchronized with the code imposed by the waveguide phase modulator in the corner station to maintain the processing gain. This can be achieved using a delay-locked loop (DLL) [8]. This is done by monitoring the difference between the half-way points of the autocorrelation of the PRN code, with a delay (τ/T_{chip}) of -1/2 and +1/2, as shown in figure 4.5. The output of this can be used to synchronize the PRN code generator at the end-station.

4.3 Technical Issues

4.3.1 Pseudo-Random Noise code and isolation

The isolation between interference signals is determined by the properties of the PRN modulation. The code's chip frequency f_{chip} determines the minimum delay difference needed for optimal isolation between reflections. The mirror separation, ΔL should satisfy $\Delta L \geq c/2f_{chip}$. The last two terms in Eq. 4 in [4] show the contamination of the M1 measurement by M2 and M3 reflections. The time average of these individual
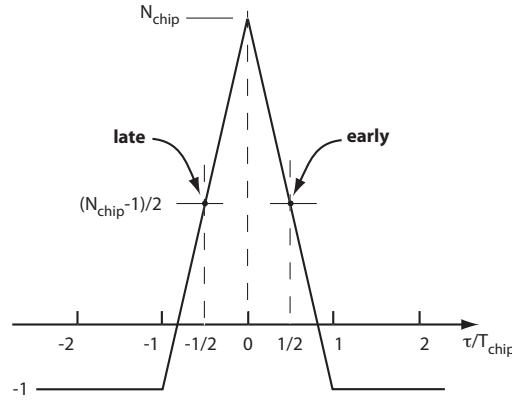
Figure 4.5: A delay-locked loop is used to synchronized the DI demodulation in the end-stations. The difference between the early and late autocorrelation, provides an error signal for synchronization of the PRN code at the end-station.

terms is similar to the code's autocorrelation with the exception that the code product is weighted by a time varying sinusoid. If the chip frequency and code frequency are not coherently related then this modified autocorrelation is approximately $2/(\pi\sqrt{n})$ for averaging over n chips.

Significantly better suppression is attainable if the heterodyne frequency f_h is an integer multiple of the chip frequency f_{chip}. In this case, each chip is weighted equally and the average is simply the code's autocorrelation. This allows for improved suppression by using PRN codes with low autocorrelation values, such as a maximal length sequence [8] whose autocorrelation is $-1/n$ for a code of n chips. In this case, the expected phase error in the measurement of M1 due to contamination from M2 is,

$$|\epsilon| \leq \frac{|E_2|}{n|E_1|} \qquad \text{rad.} \tag{4.6}$$

Arbitrarily long m-sequences are easily generated using linear feedback shift registers. A code of length 2^{14} will limit the displacement error due to crosstalk between mirror reflections to 10 pm (for $E_1 \approx E_2$). The penalty of increasing the code length is a reduction of the effective feedback bandwidth/update rate because an entire length of code must be averaged for each measurement point. With a chip frequency of 100 MHz and a code of length 2^{14} bits, the maximum measurement update rate is 6.1 kHz.

4.3.2 Phasemeter

The displacement information is extracted by a phasemeter, measuring the phase of the numerous decoded reflections. This phase difference between channels is then converted into a displacement. A simplified version of the LISA phasemeter [?] is well suited to extract the phase information. It has a displacement noise limit of $1\,\text{pm}/\sqrt{\text{Hz}}$. The LISA phasemeter is optimized for signal powers down to 1 pW and is capable of measuring 4 channels on a single FPGA. The PRN generation and decoding could be implemented by the phasemeter on the same FPGA.

Figure 4.6 shows the measured and modeled close-loop transfer function of the phasemeter. With a relative gain setting of '-10', the -3 dB point is at 552 Hz, while the phase delay at 10 Hz is -0.3 degrees.
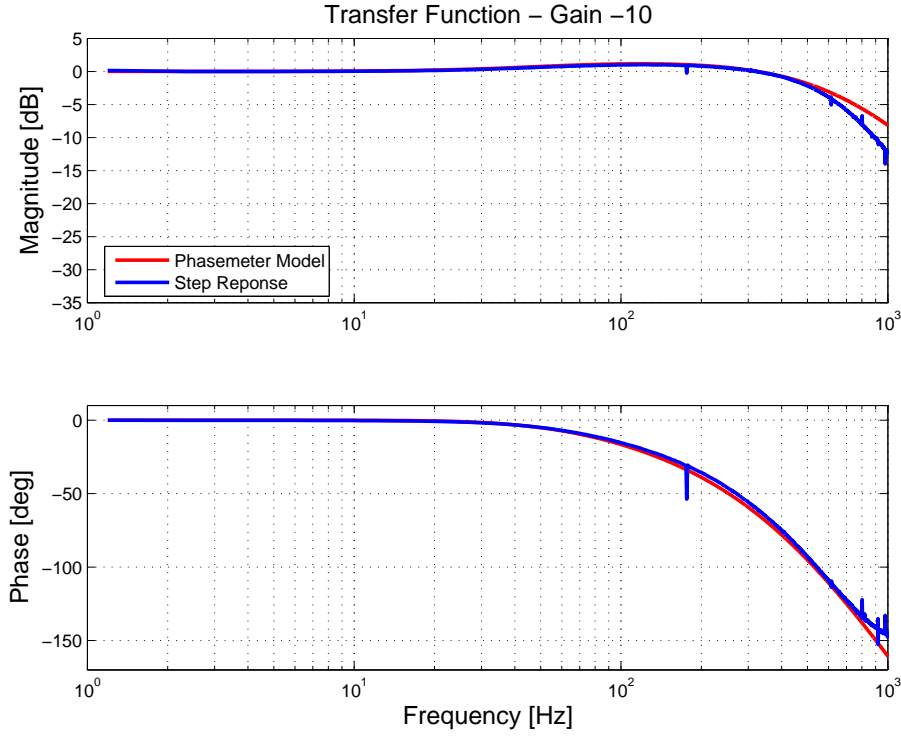

Figure 4.6: The close-loop transfer function of the phase meter with a bandwidth of 552 Hz at a nominal gain setting.

4.3.3 DI shot noise level

The DI displacement noise level is equivalent to the shot noise level conventional heterodyne interferometry. The displacement spectrum is then given by:

$$x_{DI} = \frac{\lambda}{2\pi} \sqrt{\delta\phi_{sn}^2} \qquad \mathrm{m}/\sqrt{\mathrm{Hz}} \qquad (4.7)$$

where $\delta\phi_{sn}$ is the single sided square root power phase shot noise, given by,

$$\delta\phi_{sn} = \sqrt{\frac{h\,\nu}{2P}} \qquad \mathrm{rad}/\sqrt{\mathrm{Hz}} \qquad (4.8)$$

where P is the optical power of the signal, h and ν Planck's constant and the optical frequency respectively. From figure 4.4, $P_{(n=0)} = 5$ nW resulting in $\delta\phi = 4 \times 10^{-6}$ rad/$\sqrt{\mathrm{Hz}}$. Assuming the power of the DI local oscillator (5 mW) on the DI detector is much higher then the power of the science laser (60 μW). The resulting expected displacement level is $x_{DI} = 7.3 \times 10^{-13}$ m/$\sqrt{\mathrm{Hz}}$.

4.3.4 Frequency stability

To prevent the frequency noise of the probe laser mimicking displacement noise, the DI laser frequency needs to be stabilized relative to the main IFO laser. The frequency stability requirement for the probe laser is,

$$\delta\nu < \frac{\delta x}{L}\nu \qquad \text{Hz}/\sqrt{\text{Hz}}. \tag{4.9}$$

Figure 4.7 shows the spectral density of the probe laser frequency noise limit, with respect to the PSL. The simplest way to achieve this level of stability is to phase lock
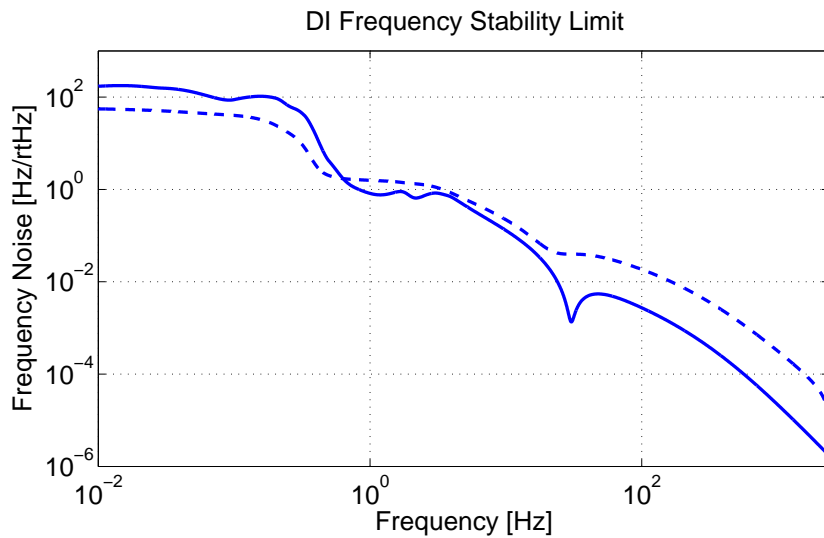

Figure 4.7: Frequency stability requirements for the DI probe laser and LO laser.

the lasers. Frequency offset phase locking is routinely performed at micro-cycle/$\sqrt{\text{Hz}}$ which is many orders of magnitude better than required.

When injecting the DI beam from within the vertex station, the probe laser can be phase locked to the PSL. A phase locking offset frequency of 1 GHz will couple in the phase noise of the 1 GHz clock. Using standard, off the shelf signal generators this noise level will be negligibly small.

In an alternative scheme where the DI beam is injected at the end station, the probe laser can be stabilized to a reference beam delivered by an optical fiber from the vertex. This reference beam is locked to the PSL and subsequently transfered to the end station by fiber. The phase noise due to the 4 km long fiber could be a significant noise source, in which case it could be cancelled using techniques described in [9].

4.3.5 Beam Pointing

There are several sources of geometrical errors due to beam pointing and optical component fluctuations. DI is a non-resonant system and so receives none of the mode filtering benefits of cavity-based sensing approaches. Using ray tracing matrices the

height and angle of the beam through the arm cavity can be tracked. The most important result of this ray tracing will be the angles of the beam after reflection off the ETM and the ITM. For are more detailed analyses see Appendix D.

In the calculations, the input beam has only an angle at the ITM. The displacement at the ITM due to the 50m optical lever arm through the recycling cavity is not included. Figure D.1 shows how the DI beam travels through the cavity, when the cavity mirrors and the input beam are tilted.
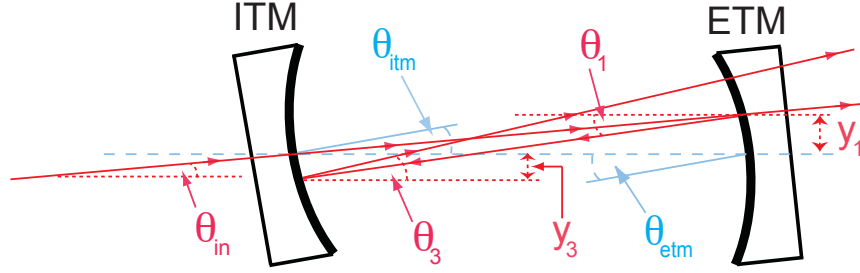

Figure 4.8: The path of the DI beam through the AdvLIGO arm cavity with tilted mirrors

The digital interferometer compares the phase of the beam that passes straight through the cavity with the one that reflects off the ETM and the ITM. The optical path length difference that results in beam pointing noise is given by:

$$x = L \left(\frac{1}{\cos\left(A\theta_{in} + 2\theta_{etm}\right)} + \frac{1}{\cos\left(B\theta_{in} + 2A\theta_{etm} + 2\theta_{itm}\right)} \right) \quad (4.10)$$

We calculate the beam pointing noise here by adding the individual optics noise contributions in quadrature. Thus the beam pointing noise is given by:

$$(\Delta x)^2 = (\Delta x_{in})^2 + (\Delta x_{etm})^2 + (\Delta x_{itm})^2 \quad (4.11)$$

Where Δx_{in}, Δx_{etm} and Δx_{itm} are the contributions to the beam pointing noise from the input beam, ETM and ITM angular noise respectively. After some differentiation, the input beam angular noise contribution to the beam pointing noise in the digital interferometer is given by:

$$\Delta x_{in} = L \left(\left(A^2 + B^2\right) \theta_{in} + 2A\left(1 + B\right)\theta_{etm} + 2\theta_{itm} \right) \Delta\theta_{in} \quad (4.12)$$

As well as for the test mass contributions, we obtain:

$$\Delta x_{etm} = L \left(2A\left(1 + B\right)\theta_{in} + 4\left(1 + A^2\right)\theta_{etm} + 4A\theta_{itm} \right) \Delta\theta_{etm} \quad (4.13)$$
$$\Delta x_{itm} = L \left(2B\theta_{in} + 4A\theta_{etm} + 4\theta_{itm} \right) \Delta\theta_{itm} \quad (4.14)$$

Where $A = \left(1 - \frac{2L}{R}\right) \approx -2.85$, and $B = \left(\frac{2L}{R}\right)^2 - 3\left(\frac{2L}{R}\right) + 1 \approx 4.27$, with $L = 3995$ m and $R = 2076$ m. The plain θ terms in equations D.22, D.23 and D.24 refer to the DC offset values of the components. In this analysis we take this to be the root mean

squared values at low frequencies of the angular noise spectra for each component. That is ~40 nrad for θ_{in} and ~110 nrad for the both θ_{itm} and θ_{etm}. The $\Delta\theta$ terms represent angular noise spectra for the input beam and the test masses, shown in figure 4.9.

Figure **??** shows the total readout displacement noise due to the above discussed jitter noise and is 3.3 nm RMS, which is to high. To over come this, a simple dither alignment feedback loop could reduce this to below the 1 nm level.
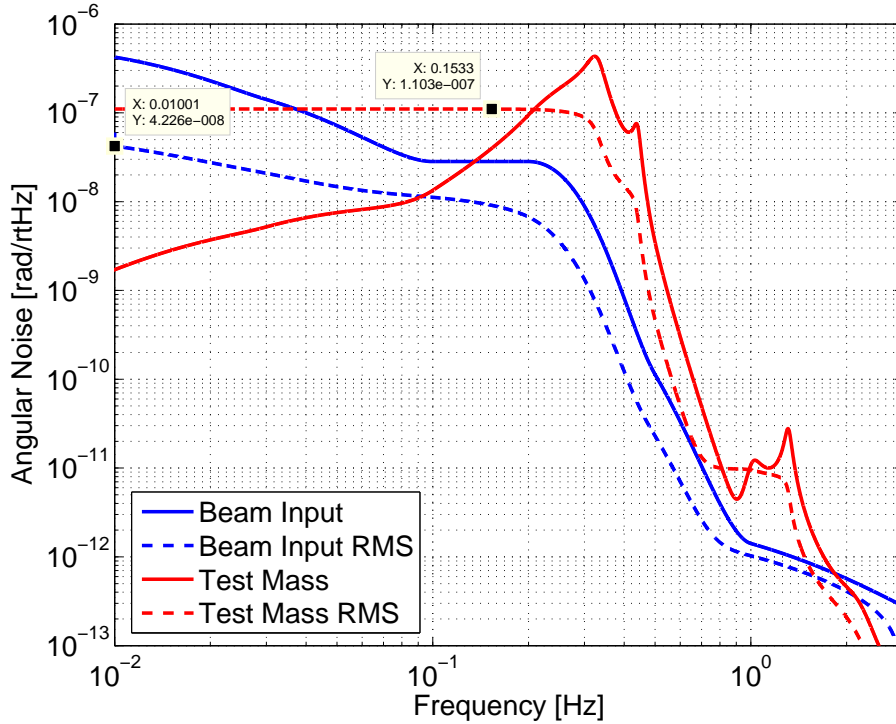

Figure 4.9: The approximated angular noise spectrum. The test mass spectra is with an active local damping (e.g. GEO based damping), while the input beam angular noise is taken to be one tenth of the HAM ISI longitudinal displacement noise.

4.3.6 Closed-loop feedback

The control signals obtained with DI will be used to stabilize the test mass position. The measured DI readout noise floor is $< 10 \text{ pm}/\sqrt{\text{Hz}}$ in the frequency range of 1 Hz to 100 Hz, with a $1/f$ slope at frequencies up to 1 Hz. To compensate for the $1/f^n$ roll-off of displacement actuators requires a f^{n-1} roll-up of controller gain. This controller roll-up will amplify the sensor noise and care must be taken to avoid saturating the displacement actuators at high frequencies.

If feedback is applied to the penultimate mass of the quad suspension the rms feedback current to each of the penultimate mass OSEMs is restricted to approximately 50 mA. This is to keep enough headroom (up to ~150 mA). Preliminary simulations of a simple feedback with only PM actuation can reach sub-nm RMS level without
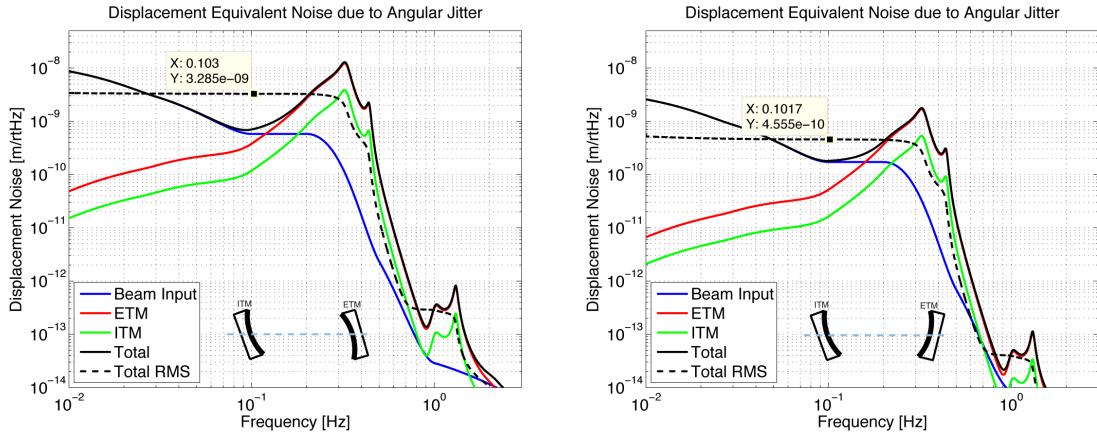
Figure 4.10: The equivalent displacement readout noise due to beam pointing noise from the input beam, ITM and ETM.

exceeding this level. A more elaborate feedback path can include feedback to the test mass as well. The electro-static drive equivalent rms force to the test mass should be kept below $\sim 20 \ \mu N$. This is to stay within a factor of $10\times$ of the maximum force ($\pm 200 \ \mu N$) achievable by the electro-static drive to be able to handle excessive excursions away from the rms value. Feedback to the platform will be difficult, as the servo response will need to include 8 zeros to compensate the quad response from the transfer function to the test mass. Which makes a servo with a 1 Hz bandwidth very difficult.

4.4 Performance

The experimental displacement noise limit for the DI is given in figure 4.11. This has been obtained by measuring the displacement noise of a 3.75 m linear cavity, which was locked using the PDH technique. The displacement noise was measured using the DI technique in transmission. Two lasers are phase locked to the each other, with a 30 kHz locking bandwidth. The main laser is split into two beams, one with phase modulator for the PDH RF sidebands, while the second is directed into a waveguide phase modulator for the DI code generation. After either modulator the beams are recombined and injected into the linear cavity. The PDH is detected in reflection, while the DI beam is detected in transmission. The second laser is then combined with the DI transmitted beam, and the beatnote is readout by the phasemeter.

The analytical curve from figure 4.11 is used as the DI noise limit in the quad feedback model. The feedback is to the test mass and the penultimate mass resulting in a residual test mass motion of 0.8 nm rms, shown in figure 4.12. In figure 4.13(a) the PM OSEM feedback current is shown, which is approximately 50 mA. In addition the feedback force to the test mass is shown in figure 4.13(b), which at 30 μN, is slightly above the max. recommended force of 20 μN.
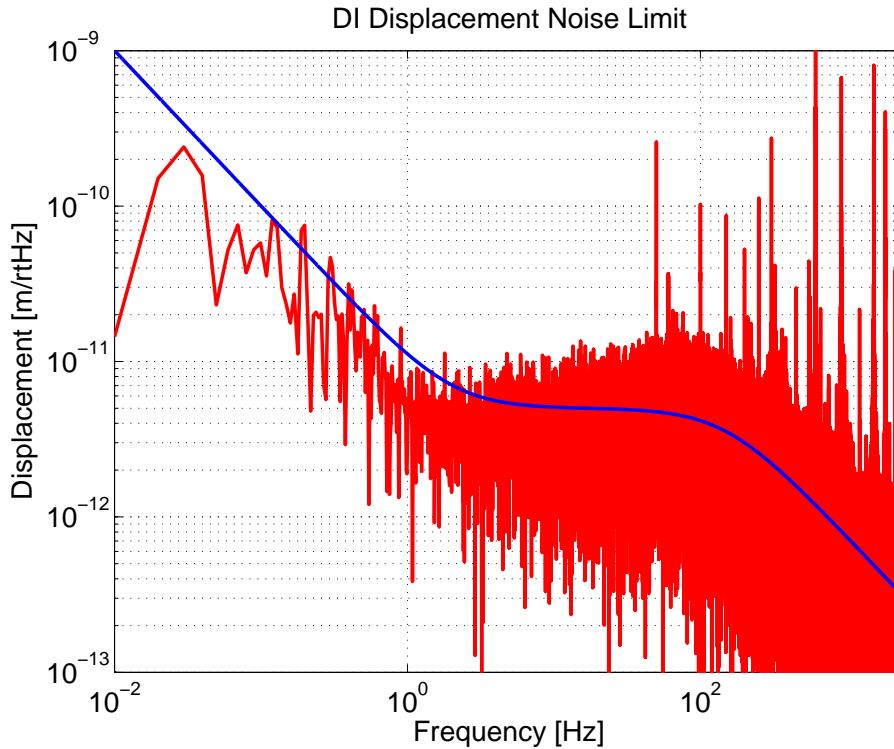
Figure 4.11: DI displacement noise limit at about $3\,\mathrm{pm}/\sqrt{\mathrm{Hz}}$ from 1 Hz to 100 Hz. The corner at ∼120 Hz is due to the bandwidth settings of the PDH servo. The zero at 1 Hz is still under investigation. The blue curve is an analytical estimate. Note: the increased noise floor below 1 Hz is not limiting the locking performance in the Quad suspension feedback simulation.

4.5 Risk Assessment

Although the displacement performance of the DI technique has been demonstrated not to be the limiting source, the technique has not been widely used.

4.6 DI Summary

The DI implementation has various benefits compared to the SPI. One advantage is that there is no major in-vacuum modification required. A few additional optics to steer the probe beam into the system, and similar for the detection of the DI probe beam in the end-stations.

In addition to the arm cavity length control, the recycling cavities (the PRM and SRM) can be readout in a similar manner. This can be done, without any additional optical components. Inside the FPGA there are more adjustable delays added, to account for each optic.

As a back up for the optical layout, the DI can be injected into the ETM in a similar manner to the Frequency shifter PDH scheme, described in the next chapter.
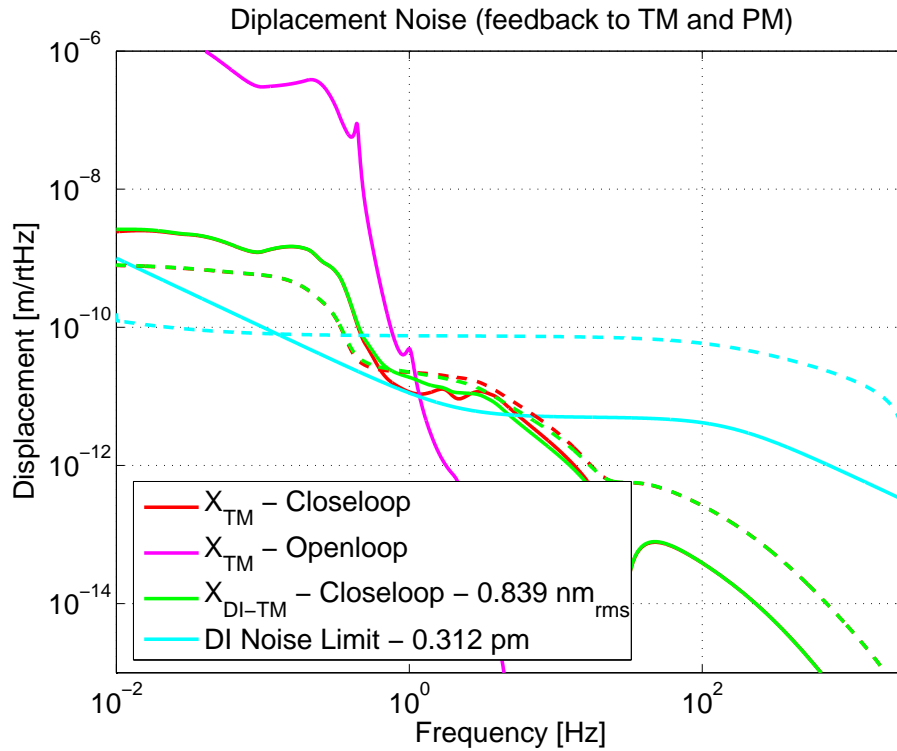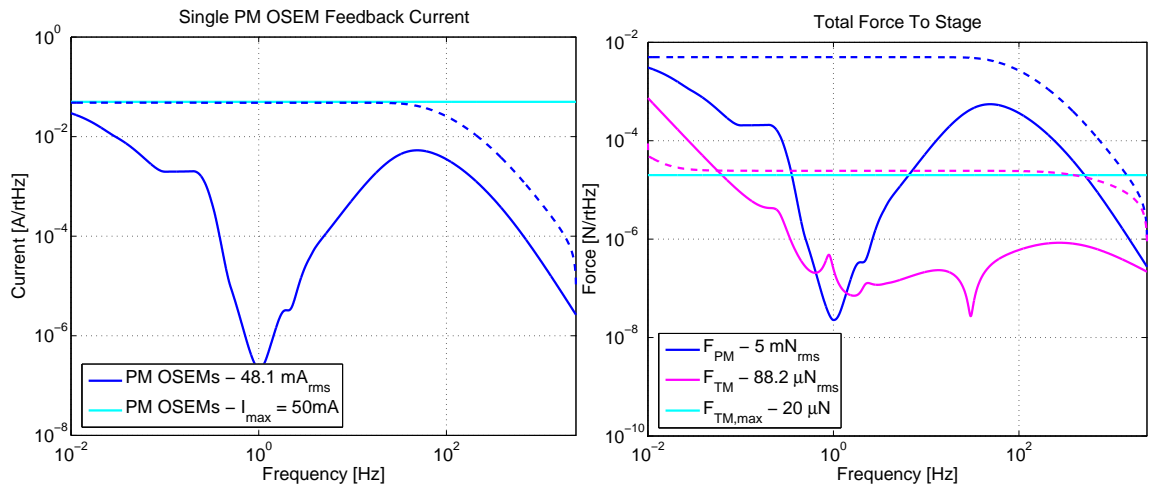
Figure 4.12: Test mass displacement noise with feedback to the penultimate mass only, using DI. The dashed lines indicate the rms value.

(a) Single OSEM feedback current.

(b) Force amplitude spectrum to the test mass and the penultimate mass.

Figure 4.13: DI feedback to the penultimate mass only. The dotted lines represent the rms values.

5 Frequency shifted PDH system

This is based on the arm cavity to be a single cavity to be locked from the end-station. A tab off from the PSL is delivered to the end-station by an optical fiber. The light is frequency shifted by a few hundred MHz using an AOM and then injected into the arm cavity with PDH sidebands. Each arm cavity will be "seen" as a single cavity, with feedback to the AOM for fast actuation and penultimate mass for guiding the arm cavity into resonance with the PSL. This is done in a similar fashion to the DI case, as the control feedback to the quad suspensions is identical. Alternatively, a dual wavelength laser (1064 nm and 532 nm), is stabilized to the PSL using the 1064 nm beam. The 532 nm output beam is used to inject into the arm cavities.

5.1 Concept and Optical Layout

The concept is to inject a second laser into the back of the arm cavities with PDH sidebands for generating an error signal. To prevent the interaction of the locked arm cavity with the power recycling cavity when trying to bring the full IFO into lock, the second laser is frequency shifted [?]. Alternatively, the PDH signal can be time tagged (using a PRN code) to isolate and average the reflected light of a coupled cavity to obtain the error signal of the cavity of interest [10]. When injecting from the end-station, the PDH signal from the arm cavity can be isolated from the cavities (PRC and SRC) in the corner station. Another approach is to use a completely different wavelength (other than 1064 nm), and modify the HR coatings on the ITM and ETM such that they will moderately reflect this second wavelength.

Preliminary modeling [?] has shown that it is possible to modify the coatings such that a second wavelength can build a moderate finesse cavity ($\sim$30), while the HR coating will be optimized for low thermal noise for 1064 nm. Using the standard 1/4-wave coating design and varying the layer thickness to optimize the reflection for the second wavelength does only degrade the 1064 nm thermal noise performance by a few percent.

Also, a beam with a wavelength of < 1026 nm transmitted through the ITM will due to the dispersion and wedge angle of the optics in the corner station, miss the ETM on return after one roundtrip in the recycling cavities (Mike Smith at CIT).

With the combination of the dispersion and coating modification, a suitable wavelength can be determined which will not interact with the cavities in the corner station. Alternatively, the coatings of the beamsplitter and the recycling cavities can be modified to be transmissive to the second wavelength. The second wavelength laser will need to be phase locked to the main PSL. Using Nd:YAG lasers (532 nm, 946 nm), then the phase locking to the PSL can be achieved quite easily. When this is not the case, a dual resonance reference cavity can be used.

Figure 5.1 shows a possible optical layout of the IFO and the layout for the secondary laser (in the enclosed rectangles). The lower rectangle shows the the sub-carrier phase locked to the PSL, and injected into an optical fiber for delivery to the end-stations. Alternatively, the PSL pick-off could be injected into the fiber, bypassing the phase lock loop. The optical circulator and fiber AOM are used in a fiber noise suppression loop. The noise due to the fiber going to the end station can be suppressed by detecting the beat between the light entering the fiber and a portion of the reflection of the light at the output of the fiber at the end station. Using a standard phase locked loop, the fiber induced noise can be suppressed to a fractional instability of $\sim 10^{-15}$ [11].

The larger rectangle in the top right corner illustrates the optical layout in the end-station. The fiber from the corner station provides the phase locked reference is injected into a local dual resonant reference cavity. This cavity is required to phase lock second wavelength laser to the PSL. That is, if the second laser is 532 nm, then this reference cavity would not be required. Once the second wavelength laser is phase locked, it will be injected into the arm cavity with PDH sideband using the phase modulator. Fast actuation is done by feeding back to the AOM to acquire lock of the laser to the arm cavity. Once this is achieved, feedback to the quad suspension can be engaged to reduce the test mass motion for interferometer lock acquisition.

5.2 Technical Issues

5.2.1 Cavity Finesse

The finesse of the

5.2.2 Displacement Sensitivity

For a linear cavity, the displacement equivalent shot noise is given by [12]:

$$\delta x = \frac{1}{8\,\mathcal{F}} \sqrt{\frac{h\,c\,\lambda}{P_{pd}}} \tag{5.1}$$

With an input power of 1 mW, a finesse $\mathcal{F} \sim 22$, the displacement noise is $\delta x \sim 8 \times 10^{-17}$ m/$\sqrt{\text{Hz}}$. That is using a 532 nm beam injected into the arm cavity from the end-station.

5.2.3 Frequency stabilized light at the end station

To stabilize the laser at the end-station, a phase reference in the end-station needs to be available. Delivering a portion of the PSL laser to the end-station via an optical fiber will be dominated by the noise of the 4 km long fiber. It has been shown that this can be suppressed [11].

This is achieved by phase locking an auxiliary laser (at 1064 nm) in the corner station to the PSL. The beam from this laser is split into two, one for each end-station. Each fiber to the end-station has an AOM to frequency shift the light and for fast frequency actuation, see figure 5.1. A portion of the light transmitted by the fiber will be sent
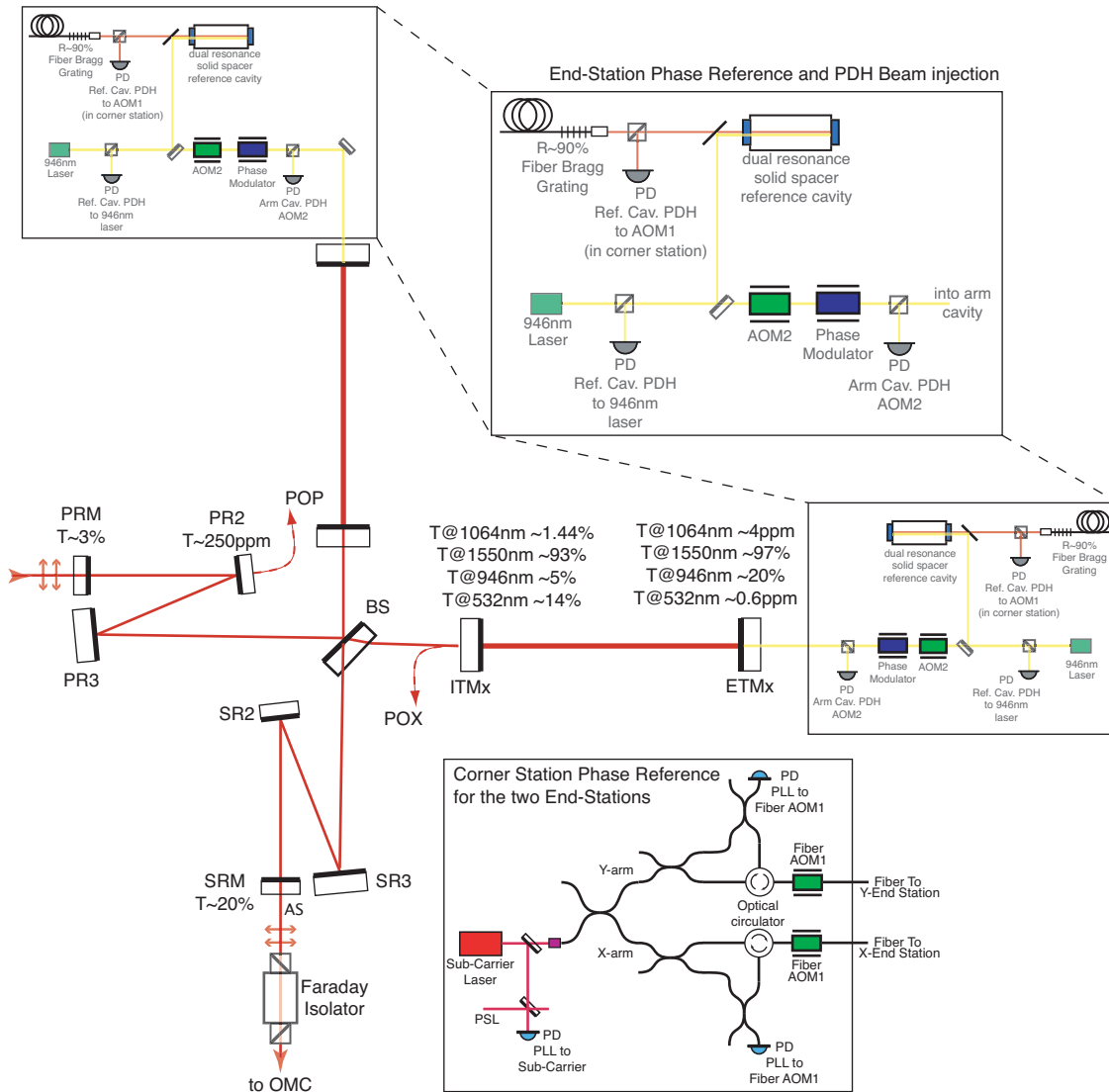
Figure 5.1: Optical layout for the PDH technique injected into the arm cavity from the ETM with a second wavelength laser.

back to the corner station and the heterodyne beatnote detected on a photo detector. Feeding back half of the phase noise measured on the beatnote to the AOM1, a copy of the phase noise which is injected into the fiber is available in the end-station, see figure 5.1.

In the end-station the light transmitted through the fiber is locked to a reference cavity. The cavity is a solid spacer, suspended reference cavity. The fiber delivered light is locked to the cavity by feeding back to AOM1 in the corner station. Alternatively, the reference cavity can have a PZT.

In the end-station a second laser at the wavelength of 946 nm, is made resonant with the reference cavity as well, by feeding back to the laser. An additional AOM is used as a frequency actuator and phase modulator is used to put the PDH phase sidebands on the laser beam before it is injected into the arm cavity.

5.2.4 Coating modifications

To isolate the single arm cavities from the recycling cavities during the IFO lock acquisition, it is preferred to use a second wavelength. Currently a wavelength of 946 nm is assumed. A few initial reasons are 946 nm is available from a solid-state Nd:YAG laser, which provides a free running laser linewidth of $< kHz$. In addition when looking at the ETM high reflective coating, there is a slightly elevated reflectivity at 946 nm. This can be explored to make this wavelength more reflective $\sim 80\%$ without compromising the thermal noise performance of the coating at 1064 nm (within a few %). Alternatively, a wavelength of 532 nm can be used, which will greatly simplify the phase locking to the PSL, by using a dual wavelength laser.

5.3 Performance

Figure 5.4 shows the test mass displacement with the frequency shifted PDH system, feeding back to the penultimate mass. Because of the lower noise limit of the PDH technique (compared to the DI case), it is possible to reduce the test mass displacement without the possibility of saturating the actuators.
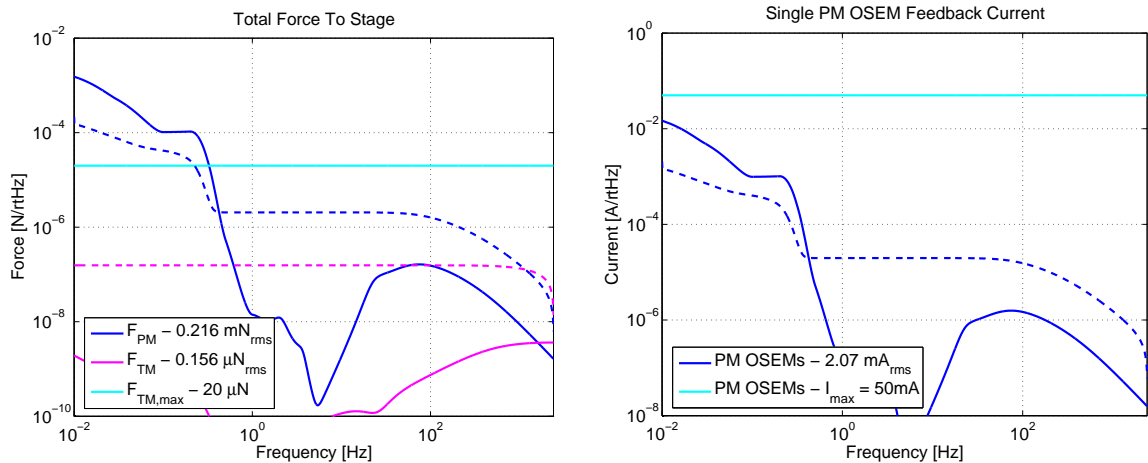
(a) Force amplitude spectrum to the test mass (implied) and the penultimate mass (actual).

(b) Single OSEM feedback current.

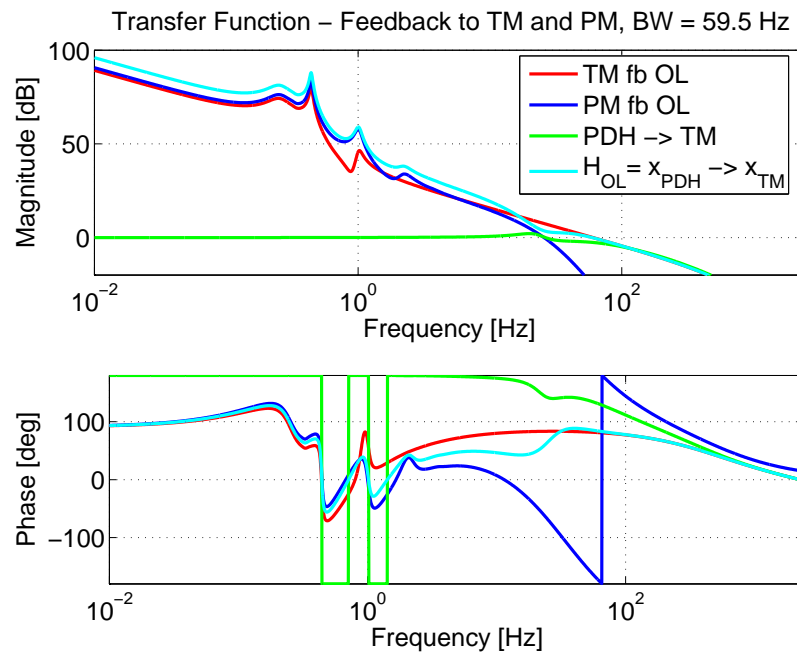Figure 5.2: Feedback to the penultimate mass only. The dotted lines represent the rms values.

Figure 5.3: Servo feedback transfer functions, with the PDH readout technique.
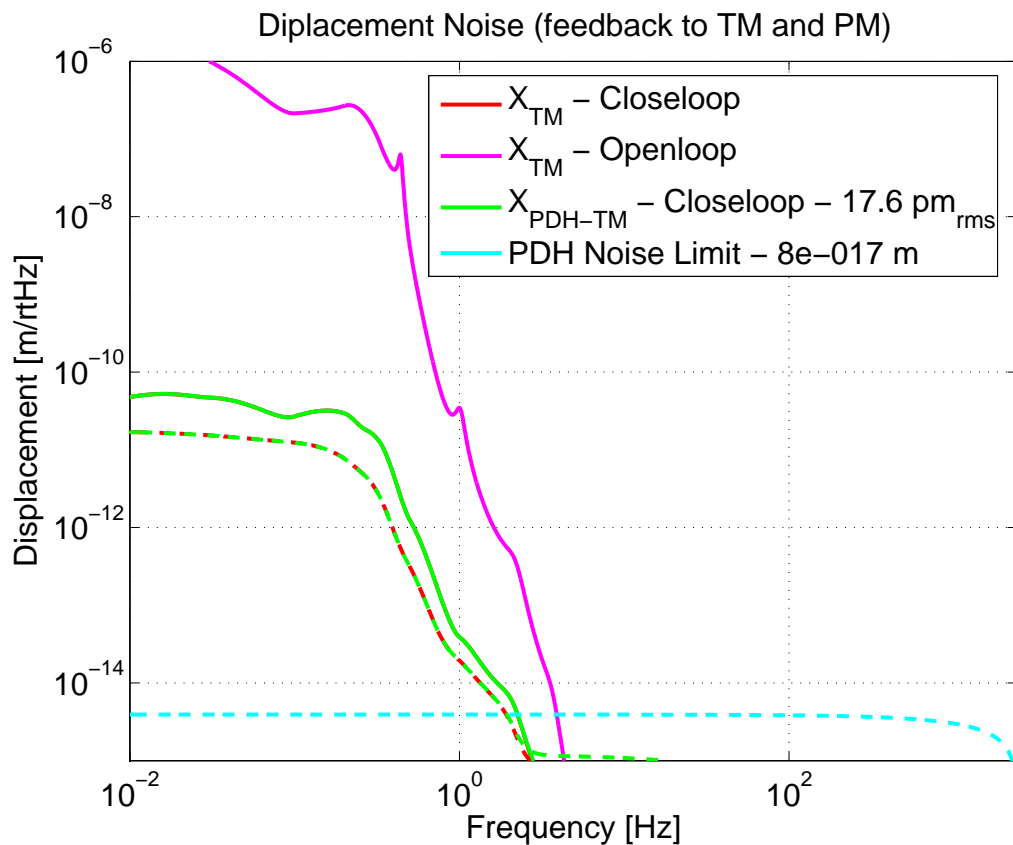

Figure 5.4: Test mass displacement noise with feedback to the penultimate mass only. The PDH noise floor is at 8×10^{-17} m/$\sqrt{\text{Hz}}$ with 1mW of incident light at 946 nm. The dashed lines indicate the rms value.

6 Recommendations

All techniques presented in the paper can do the task outlined in section 1.2. The SPI is the most mechanical intervention of the 3 provided solutions. In the other hand it is a simple solution, especially when the injection is done from the end-stations. A drawback is that the test mass displacement (location) is inferred. This in contrast to the other two solutions, which directly measure the test mass displacement. The DI approach is a recently developed technique to be implemented in LISA. It provides a direct displacement readout without calibration. As well it has a potential advantage that it can measure the displacement/location of all the core optics of the IFO, providing the ability to place each optic at a designated location. The Frequency shifter PDH technique has the advantage of being a straight forward technique on which LIGO has been running for years. It has a low noise floor, even with little power, reducing the strain on the suspension actuators. In the other hand there are multiple control loops per system to obtain a working system. Table 6.1 summarized the three options and some key difference.

Table 6.1: Summary of the solutions.

Solution	Invasive	Test Mass Noise level	Key modifications	Wavelength	Advantages
SPI-end injection	moderate	10^{-9} m/$\sqrt{\text{Hz}}$	second suspension from the ISI	1064/532 nm	running during science mode
DI	minor	10^{-11} m/$\sqrt{\text{Hz}}$	use of output FI and DI/carrier separation	1064 nm	sensing of all core optics
PDH	minor	10^{-14} m/$\sqrt{\text{Hz}}$	HR coatings	532/964 nm	established

In appendix C an alternative injection for the DI and PDH technique is discussed. The key benefit is that all the injection and detection is done in the corner station. Also, to prevent spurious reflections/interference from 'to other cavity', the beamsplitter and optics in the recycling cavities are to be made transmissive to the used wavelength.

6.1 Issues to be Addressed

6.1.1 SPI

SPI Input Optics/Mode-Matching, where to place the various steering mirrors and other optical components in the vacuum system (HAM3 etc.). This can potentially be overcome by injecting from the end-station.

34

6.1.2 DI

Pointing, investigate the pointing of the probe beam at the faraday isolator to the ETM detection bench.

Code reflections, investigate how the 'pulses' travel through the interferometer. This needs to be done in a time domain model (e2e).

6.1.3 PDH

Stabilization of fiber noise, although this has been addressed by Ye [11] some experiments will need to be performed to copy a PSL phase reference to the end-stations.

Dual resonant Reference Cavity, is required when a (non 532 nm) second wavelength is used. This reference cavity will be resonant for the 1064 nm and the second wavelength, to lock the second laser to the PSL.

Second Wavelength, needs to be determined. When 532 nm is used the frequency stabilization can be simply implanted by using a double 1064 nm output.

A Change Notice

A.1 Version T080139_00_I_11July08

This list the changes made since version T080139_00_I_04June08.

1. Modified the sections in the Change Notice, to reflect the relevant version instead of reffering to the previous version.

2. moved the **Change Notice** to be the appendix A.

3. improved and updated section **4.3.5 Beam Pointing** in the DI scheme.

4. included the more detailed DI Beam Pointing done by Adam in the appendix D.

5. included the phasemeter close-loop transfer function in section 4.3.2.

A.2 Version T080139_00_I_04June08

This list the changes made since version wp02June08.

1. started to include a change notice list.

2. moved section **4.1.1 Displacement Noise Limit** to the start of section **4.4 Performance**.

3. modified caption of figure 4.11 from 'The corner at ∼120 Hz is due to the bandwidth settings of the phasemeter.' → 'The corner at ∼120 Hz is due to the bandwidth settings of the PDH servo.'

4. fixed LIGO-T060303 reference in section **4.2.2 Back-scatter at the AS port**.

5. extended section **Back-scatter at the AS port** with - In addition a retractable steering mirror before the beam dump at the beam splitter port can be used to remove the DI beam entering the AS-port when in science mode.

6. modified figure 4.3 to include a retractable mirror at the AS port.

7. adjusted some numbers in the paragraph after equation 4.6, changed 5 pm to 10 pm and 100 kHz to 6.1 kHz.

8. corrected equation 4.7.

9. changed wording in the paragraph after 4.8.

10. replaced the two sentences after equation 4.9, with 'Figure 4.7 shows the spectral density of the probe laser frequency noise limit, with respect to the PSL.'

11. rewrote the paragraph after equation 4.3.5, removed the numbers.

12. modified the last paragraph of section **4.4 Performance**.

13. modified figure C.1 to include the optimised coating transmission using Stefan's code.

B Quad-Suspension Feedback Servo Implementation

The feedback to the quad-suspension is done by feeding back to the test mass (TM) and/or penultimate mass (PM). The transfer function from the force to the TM to the TM displacement has a $1/f^2$ frequency dependency. Also, the PM force to TM displacement transfer function has a $1/f^4$ frequency dependency. In the PM servo, the response will have a pole at a low frequency, and 4 zeros to compensate the $1/f^4$ response to make a stable control loop. Due to the quad suspension resonances, which will be within servo bandwidth, the control loop will be tricky.
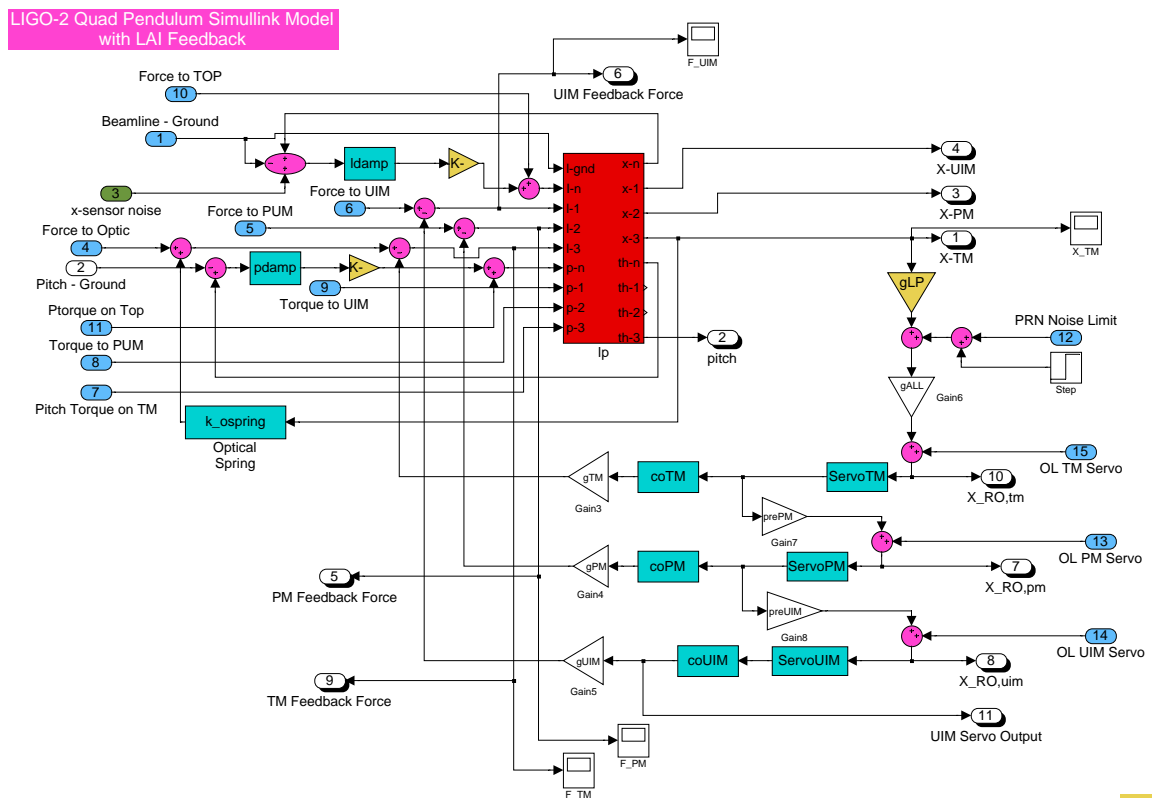

Figure B.1: The simulink model.

To stop the servo response going up by f^4, a 4th order low-pass cut-off filter is used with a corner frequency of ~ 32 Hz. The location of the corner frequency has a strong influence in the resulting rms OSEM current. Setting this to low will eat away to much phase margin at the lower frequencies for a stable feedback servo loop.

Figure B.1 shows the simulink model used to generate the displacement and transfer function figures.

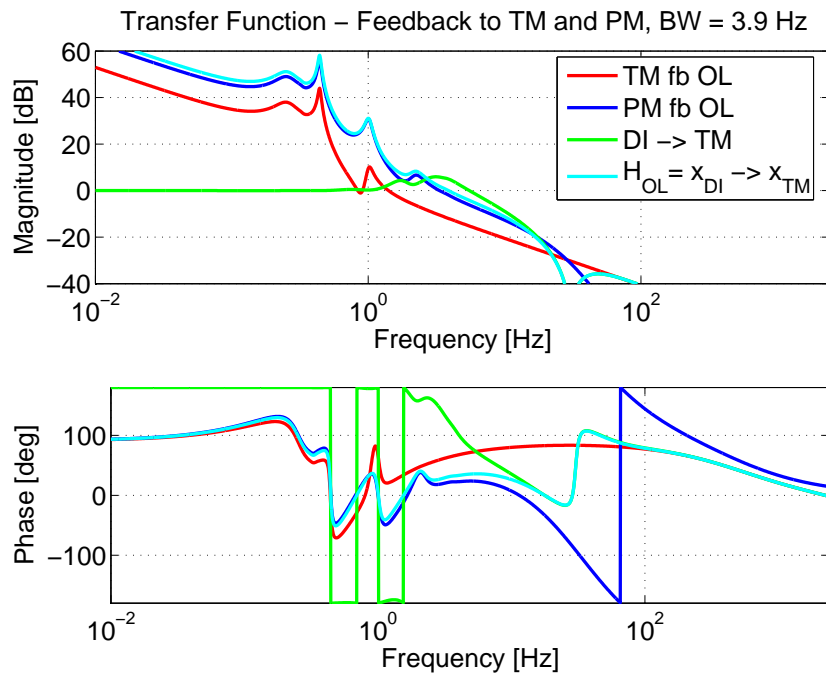Figure B.2 shows the open-loop feedback transfer function.

Figure B.2: DI servo transfer functions, UGF = 3.9 Hz with a phase margin of 32 deg.

C Alternative Injection

An alternative injection of the DI beam in the interferometer is shown in figure C.1. The basic DI readout will be done in reflection as the DI beam will have a high transmission through the ITMs and ETMs. This results in comparable amplitude reflections from the ITM and ETM on the DI readout detector. The major advantage is that all injection and detection is done in the corner station.

The DI wavelength is chosen to be 946/1319/1550 nm to comply with the waveguide phase modulator. Each arm cavity will have its own DI injection beam, injected from the 3rd recycling cavity mirror. To eliminate any coupled cavity effects, the SR3 (and PR3) and beamsplitter have a modified coating to minimize the reflectivity at the DI wavelength. Alternatively, the injection can also be done in the second recycling mirrors (PR2/SR2) instead.

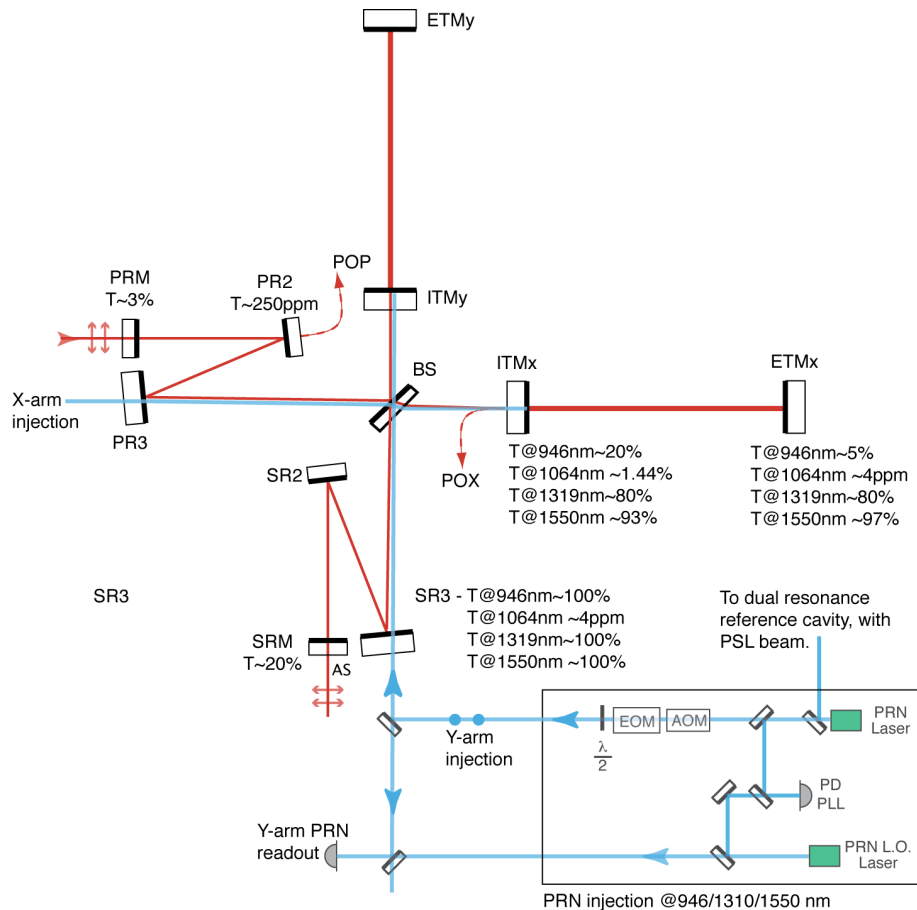In the other hand, the same beam path can be used with the PDH approach.

Figure C.1: Alternative DI injection (can also be used with the PDH approach).

D Beam Pointing Noise in the Digital Interferometer

D.1 Introduction

Jitter of the Digital Interferometer input beam and the cavity optics couples into the readout of the cavity displacement by changing the optical path length of the beam. This document describes and calculates how the jitter couples in and the displacement equivalent noise it adds to the DI readout of the AdvLIGO arm cavities. For the rest of this document we will refer to this displacement equivalent noise as Beam Pointing Noise.

D.2 Ray Tracing

Using ray tracing matrices we can track the height and angle of the beam through the arm cavity. The most important result of this ray tracing will be the angles of the beam after reflection off the ETM and the ITM.

In the calculations, the input beam has only an angle at the ITM. The displacement at the ITM due to the 50m optical lever arm through the recycling cavity is not included. Figure D.1 shows how the DI beam travels through the cavity, when the cavity mirrors and the input beam are tilted.
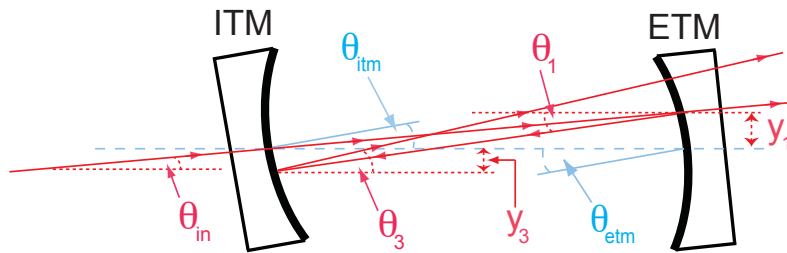

Figure D.1: The path of the PRN beam through the AdvLIGO arm cavity with tilted mirrors

The following equation gives the height and angle of the beam relative to a horizontal axis through the centre of the mirrors, just before it reflects off the ETM. The lateral beam displacement due to the tilting of the ITM is negligible, and as such is not included.

$$\begin{pmatrix} y_0 \\ \theta_0 \end{pmatrix} = \begin{pmatrix} 1 & L \\ 0 & 1 \end{pmatrix} \begin{pmatrix} 0 \\ \theta_{in} \end{pmatrix} = \begin{pmatrix} L\theta_{in} \\ \theta_{in} \end{pmatrix} \tag{D.1}$$

Where $L = 3995m$ is the length of the cavity and θ_{in} is the angle of the beam entering the cavity. The next equation gives the height and angle of the beam reflected off the ETM.

$$\begin{pmatrix} y_1 \\ \theta_1 \end{pmatrix} = \begin{pmatrix} 1 & 0 \\ \frac{-2}{L} & 1 \end{pmatrix} \begin{pmatrix} y_0 \\ \theta_0 + 2\theta_{etm} \end{pmatrix} = \begin{pmatrix} L\theta_{in} \\ \left(1 - \frac{2L}{R}\right)\theta_{in} + 2\theta_{etm} \end{pmatrix} \tag{D.2}$$

Where $R = 2076m$ is the radius of curvature for both ITM and ETM, and θ_{etm} is the angle of the ETM to the horizontal axis. Note that θ_{etm} is positive when the mirror normal is above the axis, in defiance of the usual clockwise equals positive convention. The next equation gives the height and angle of the beam before it reflects off the ITM.

$$\begin{pmatrix} y_2 \\ \theta_2 \end{pmatrix} = \begin{pmatrix} 1 & L \\ 0 & 1 \end{pmatrix} \begin{pmatrix} y_1 \\ \theta_1 \end{pmatrix} = \begin{pmatrix} 2L\left(1 - \frac{L}{R}\right)\theta_{in} + 2L\theta_{etm} \\ \left(1 - \frac{2L}{R}\right)\theta_{in} + 2\theta_{etm} \end{pmatrix} \tag{D.3}$$

Finally this equation gives us the height and angle of the beam after it reflects off the ITM.

$$\begin{pmatrix} y_3 \\ \theta_3 \end{pmatrix} = \begin{pmatrix} 1 & 0 \\ \frac{-2}{L} & 1 \end{pmatrix} \begin{pmatrix} y_2 \\ \theta_2 + 2\theta_{itm} \end{pmatrix} = \begin{pmatrix} 2L\left(1 - \frac{L}{R}\right)\theta_{in} + 2L\theta_{etm} \\ \left(\left(\frac{2L}{R}\right)^2 - 3\left(\frac{2L}{R}\right) + 1\right)\theta_{in} + 2\left(1 - \frac{2L}{R}\right)\theta_{etm} + 2\theta_{itm} \end{pmatrix} \tag{D.4}$$

Where θ_{itm} is the angle of the ITM. The important results from this ray tracing are the angles of the beam after reflection off each test mass, that is θ_1 and θ_3.

$$\theta_1 = A\theta_{in} + 2\theta_{etm} \tag{D.5}$$
$$\theta_3 = B\theta_{in} + 2A\theta_{etm} + 2\theta_{itm} \tag{D.6}$$

Where A and B are given by:

$$A = \left(1 - \frac{2L}{R}\right) \approx -2.85 \tag{D.7}$$

$$B = \left(\frac{2L}{R}\right)^2 - 3\left(\frac{2L}{R}\right) + 1 \approx 4.27 \tag{D.8}$$

D.3 Difference in Optical Path Length

The difference in optical path length of the beam from the ITM to the ETM, due to the tilting of the input beam can easily be shown to equal:

$$x_0 = \frac{L}{\cos\theta_{in}} - L \tag{D.9}$$

And the difference in the optical path length due to the tilted ITM and ETM as well as the tilted beam is given by:

$$x_1 = \left(\frac{L}{\cos\theta_{in}} - L\right) + \left(\frac{L}{\cos\theta_1} - L\right) + \left(\frac{L}{\cos\theta_3} - L\right) \tag{D.10}$$

The digital interferometer compares the phase of the beam that passes straight through the cavity with the one that reflects off the ETM and the ITM. The path length difference x_0 is common, and therefore isn't readout by the digital interferometer. The optical path length difference that results in beam pointing noise is given by:

$$x \quad = \quad x_1 - x_0 = L \left(\frac{1}{\cos \theta_1} + \frac{1}{\cos \theta_3} - 2 \right) \tag{D.11}$$

$$x \quad = \quad L \left(\frac{1}{\cos \left(A\theta_{in} + 2\theta_{etm} \right)} + \frac{1}{\cos \left(B\theta_{in} + 2A\theta_{etm} + 2\theta_{itm} \right)} \right) \tag{D.12}$$

D.4 Beam Pointing Noise

We calculate the beam pointing noise here by adding the individual optics noise contributions in quadrature. Thus the beam pointing noise is given by:

$$(\Delta x)^2 = (\Delta x_{in})^2 + (\Delta x_{etm})^2 + (\Delta x_{itm})^2 \tag{D.13}$$

Where Δx_{in}, Δx_{etm} and Δx_{itm} are the contributions to the beam pointing noise from the input beam, ETM and ITM angular noise respectively. We also make the assumption that the beam pointing noise is linear to the angular fluctuations that cause it. This assumption is valid provided the fluctuations are small enough (NEED A BETTER VALIDITY COND HERE). Therefore each noise contribution is calculated by multiplying its partial derivative of the optical path length difference (equation D.12) by its angular noise. Therefore:

$$\Delta x_{in} \quad = \quad \left(\frac{\partial x}{\partial \theta_{in}} \right) \Delta \theta_{in} \tag{D.14}$$

$$\Delta x_{etm} \quad = \quad \left(\frac{\partial x}{\partial \theta_{etm}} \right) \Delta \theta_{etm} \tag{D.15}$$

$$\Delta x_{itm} \quad = \quad \left(\frac{\partial x}{\partial \theta_{itm}} \right) \Delta \theta_{itm} \tag{D.16}$$

$$\tag{D.17}$$

Where the $\Delta\theta$ terms represent angular noise spectra for the input beam and the test masses. The partial derivatives are easily calculated using the chain rule. For example we calculate the partial derivative with respect to the input beam angle in the following way:

$$\frac{\partial x}{\partial \theta_{in}} \quad = \quad \frac{\partial x}{\partial \theta_1} \frac{\partial \theta_1}{\partial \theta_{in}} + \frac{\partial x}{\partial \theta_3} \frac{\partial \theta_3}{\partial \theta_{in}} \tag{D.18}$$

$$= \quad L \left(\frac{A \sin \theta_1}{\cos^2 \theta_1} + \frac{B \sin \theta_3}{\cos^2 \theta_3} \right) \tag{D.19}$$

We then use the small angle approximation to simplify the above and get:

$$\frac{\partial x}{\partial \theta_{in}} = L\left(A\theta_1 + B\theta_3\right) \tag{D.20}$$

Substituting equations D.5 and D.6 into the above we obtain:

$$\frac{\partial x}{\partial \theta_{in}} = L\left(\left(A^2 + B^2\right)\theta_{in} + 2A\left(1 + B\right)\theta_{etm} + 2\theta_{itm}\right) \tag{D.21}$$

Therefore the input beam angular noise contribution to the beam pointing noise in the digital interferometer is given by:

$$\Delta x_{in} = L\left(\left(A^2 + B^2\right)\theta_{in} + 2A\left(1 + B\right)\theta_{etm} + 2\theta_{itm}\right)\Delta\theta_{in} \tag{D.22}$$

Using the same method for the test mass contributions, we obtain:

$$\Delta x_{etm} = L\left(2A\left(1 + B\right)\theta_{in} + 4\left(1 + A^2\right)\theta_{etm} + 4A\theta_{itm}\right)\Delta\theta_{etm} \tag{D.23}$$
$$\Delta x_{itm} = L\left(2B\theta_{in} + 4A\theta_{etm} + 4\theta_{itm}\right)\Delta\theta_{itm} \tag{D.24}$$

The plain θ terms in equations D.22, D.23 and D.24 refer to the DC offset values of the components. In this analysis we take this to be the root mean squared values at low frequencies of the angular noise spectra for each component.

The angular noise spectrum of the cavity input beam is assumed to be the same as the rotational noise of the HAM ISI. This approximation is used because the DI beam is injected at the output faraday isolator which is mounted on the HAM ISI table. The rotational noise of the HAM ISI is obtained by dividing the longitudinal displacement noise requirement of the HAM ISI by a factor of ten. This noise spectrum can be seen in figure D.2. The RMS value at low frequencies is 40nrad.

The longitudinal to pitch coupling of the quadruple suspension system is believed to be the dominant contribution to the angular noise for the test masses. As such the angular noise spectrum for ETM and ITM is calculated by multiplying the longitudinal to pitch transfer function of the quad system by the displacement noise spectrum of the HAM BSC. This spectrum can be seen in figure **??**. The RMS value at low frequencies is 120nrad.

The negative coefficients of the θ_{etm} terms in equations D.22, D.23 and D.24, means that if the DC offset of the ETM has the same polarity as that of the ITM and the input beam, then it will reduce the beam pointing noise. However, we are more concerned with the maximum noise, so we use a negative offset for the ETM.

Substituting these noise spectra and DC offsets into equations D.22, D.23 and D.24 we obtain the beam pointing noise contributions from the input beam and test masses. And by adding these contributions in quadrature as in accordance with equation D.13 we obtain the total beam pointing noise in the DI readout of the arm cavities. These noise spectra can be seen in figure D.3. The maximum noise is approximately 14nrad/$\sqrt{Hz}$ a factor of fourteen above the limit set for the digital interferometer
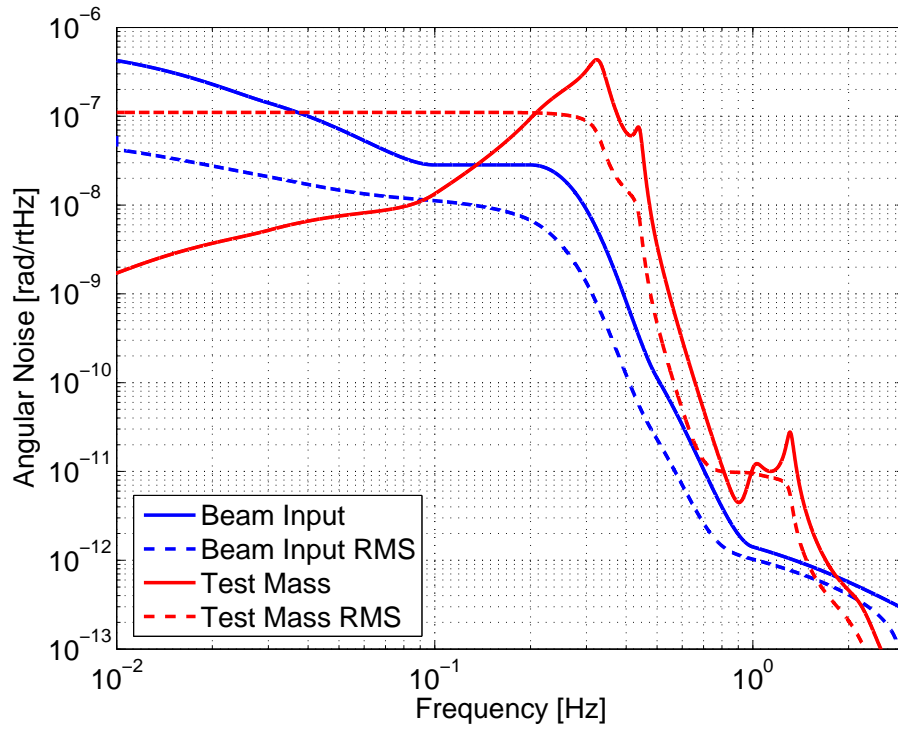
Figure D.2: The approximated angular noise spectrum of the cavity input beam. Taken to be one tenth of the HAM 4 displacement noise. The ITM and ETM angular noise are calculated from the longitudinal to pitch coupling of the quadruple suspension system and the displacement noise of the HAM BSC

scheme.

Its worth noting that the offsets of the test masses are set for a worst case scenario. But by controlling these offsets via some dither locking scheme we can lower the beam pointing noise to the desired level.
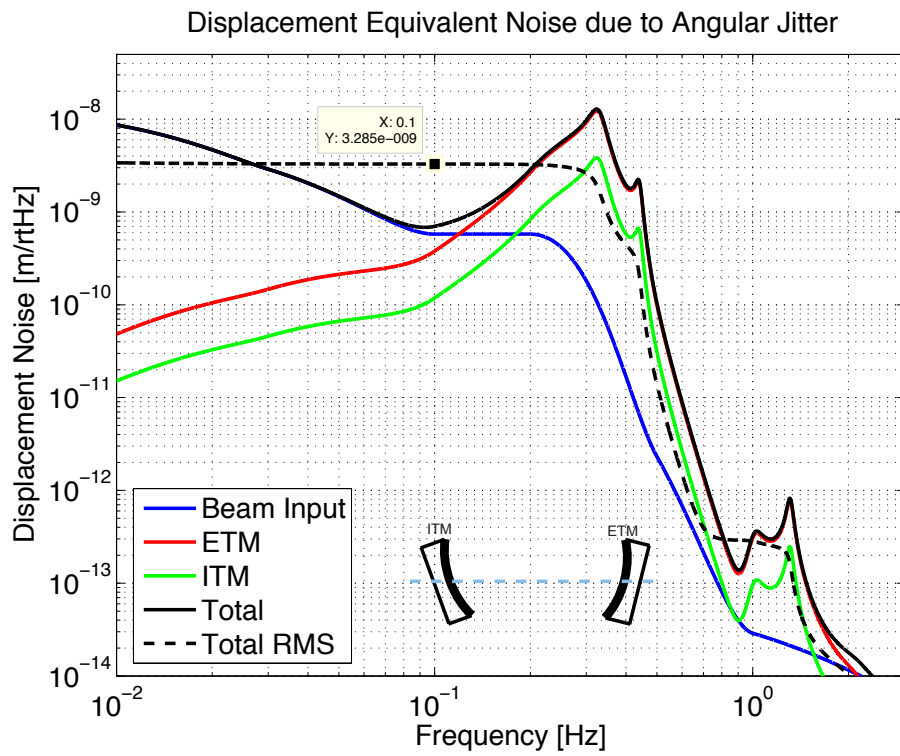
Figure D.3: The beam pointing noise from the input beam, ETM and ITM, and the total beam pointing noise spectrum

Bibliography

[1] Osamu Miyakawa and Hiroaki Yamamoto. Modeling of AdLIGO arm lock acquisition using E2E time domain simulation. *LIGO-G070129-00-Z*, 2007.

[2] Rich Abbott, Rana Adhikari, Stefan Ballmer, Lisa Barsotti, Matt Evans, Peter Fritschel, Valera Frolov, Guido Mueller, Bram Slagmolen, and Sam Waldman. AdvLIGO Interferometer Sensing and Control Conceptual Design. *LIGO-T070247-00-I*, February 2008.

[3] Ronald W P Drever and Steven J Augst. Extension of gravity-wave interferometer operation to low frequencies. *Class. Quantum Grav.*, 19:2005–2011, 2002.

[4] Daniel A. Shaddock. Digitally enhanced heterodyne interferometry. *Opt. Lett.*, 32(22):3355–3357, 2007.

[5] R. W. P. Drever, J. L. Hall, F. V. Kowalski, J. Hough, G. M. Ford, A. J. Munley, and H. Ward. Laser phase and frequency stabilization using an optical resonator. *Appl. Phys. B*, 31:97, 1983.

[6] M. Evans. SPI Model. *http://ilog.ligo-wa.caltech.edu:7285/advligo/SPI_SPI*, March 2008.

[7] P. Fritschel. Backscattering from the AS port: Enhanced and Advanced LIGO. Ligo-t060303-00-d, LIGO, December 2006.

[8] J. Meel. Spread spectrum - introduction. Technical report, De Nayer Institute, http://www.sss-mag.com/ss01.html, Oct 1999.

[9] Seth M. Foreman, Kevin W. Holman, Darren D. Hudson, David J. Jones, and Jun Ye. Remote transfer of ultrastable frequency references via fiber networks. *Review of Scientific Instruments*, 78(2):021101, 2007.

[10] Philip Graff and Sam Waldman. Time-variable interferometry for ligo lock acquisition. Technical Report 00, LIGO, August 2007.

[11] Jun Ye, Jin-Long Peng, R. Jason Jones, Kevin W. Holman, John L. Hall, David J. Jones, Scott A. Diddams, John Kitching, Sebastien Bize, James C. Bergquist, Leo W. Hollberg, Lennart Robertsson, and Long-Sheng Ma. Delivery of high-stability optical and microwave frequency standards over an optical fiber network. *J. Opt. Soc. Am. B*, 20(7):1459–1467, 2003.

[12] ERIC D. BLACK. AN INTRODUCTION TO POUND–DREVER–HALL LASER FREQUENCY STABILIZATION. *American Journal of Physics*, 69(1):79–87, 2001.